Research Square

Preprints are preliminary reports that have not undergone peer review.
They should not be considered conclusive, used to inform clinical practice,
or referenced by the media as validated information.

Delayed-Memory Dynamics of Rock-Mass Instability During TBM Metro Tunnel Excavation

Srđan Kostić

srdjan.kostic@jcerni.rs

Jaroslav Černi Water Institute

Research Article

Keywords: TBM excavation, metro tunnels, rock-mass instability, nonlinear dynamics, delayed interaction, memory-dependent weakening

Posted Date: August 31st, 2026

DOI: https://doi.org/10.21203/rs.3.rs-10562325/v1

License: This work is licensed under a Creative Commons Attribution 4.0 International License.
Read Full License

Additional Declarations: No competing interests reported.

Delayed-Memory Dynamics of Rock-Mass Instability During TBM Metro Tunnel Excavation

Corresponding author: Srđan Kostić[1,2]; srdjan.kostic@jcerni.rs

1 Jaroslav Černi Water Institute, Serbia

2 University of Novi Sad, Faculty of Technical Science, Serbia

Keywords: TBM excavation; metro tunnels; rock-mass instability; nonlinear dynamics; delayed interaction; memory-dependent weakening

Abstract

Tunnel boring machine (TBM) excavation in jointed and faulted rock may produce delayed fracture activation, intermittent slip, and spatially migrating microseismic activity that are difficult to interpret solely from quasi-static excavation stages. This study develops a reduced-order nonlinear model in which the advancing TBM face acts as a moving mechanical perturbation on two coupled rock domains. The formulation combines nonlinear friction, delayed inter-domain interaction, a slowly evolving memory variable representing cumulative weakening, and optional stochastic heterogeneity. Numerical simulations identify stable, selectively activated, and coupled stick-slip regimes. The near-critical baseline exhibits delayed clustered events after local face passage, while parameter sweeps reveal sharp two-stage transitions in which the downstream domain activates before the full coupled system. TBM advance rate has a non-monotonic effect: slow advance promotes memory-dominated instability, intermediate rates create a narrow stabilization window, and rapid advance produces near-face impulsive activation. Delay, memory accumulation, memory relaxation, and memory-dependent friction sensitivity jointly control the transition boundaries. The model is not intended to replace continuum or discontinuum analyses, but to complement them by isolating temporal mechanisms governing delayed instability. The results provide testable hypotheses for interpreting event localization, post-passage activity, and precursor patterns in TBM monitoring of structurally controlled rock masses.

1. Introduction

1.1 Dynamic response of rock masses during TBM excavation

Tunnel boring machines (TBMs) are widely used for the construction of metro, railway, hydropower and utility tunnels because they provide continuous excavation, a regular excavation profile and comparatively limited disturbance outside the immediate excavation zone. Nevertheless, the response of the surrounding ground may become complex where a tunnel alignment crosses strong, brittle, jointed or faulted rock under a non-uniform in situ stress field. In such settings, face advance produces a moving pattern of unloading and stress concentration, while cutter action, shield contact, gripper loading

and support installation introduce additional mechanical disturbances. The resulting response may include progressive cracking, spalling, block detachment, convergence, slip along discontinuities and low-energy microseismic activity. Under high-stress conditions, these processes may develop into strainburst or fault-slip rockburst phenomena [1, 8, 9].

The relevance of these phenomena to metro construction requires careful qualification. Many urban metro tunnels are shallow and are excavated in soil, weak rock or mixed-face conditions, where settlement, face stability, ground loss and interaction with existing structures are generally more important than excavation-induced seismicity. The present study is therefore directed specifically toward metro tunnel sections located in competent, fractured or tectonically disturbed rock, and toward cases in which the advancing TBM interacts with discrete structural features. Within this domain, even events of small magnitude can be operationally important because they may be associated with local overbreak, shield jamming, cutter damage, instability behind the face or sudden activation of a weak zone.

Field monitoring has shown that microseismic activity around deep tunnels is closely related to excavation advance and that concentrations of events in space and time may precede local instability [4, 9]. Geological structures can strongly modify this response by localizing stress transfer and providing surfaces for intermittent slip. A documented fault-slip rockburst in a deep TBM tunnel, for example, evolved through a sequence of changing microseismic event rates, energy release and repeated post-event activation, demonstrating that the response of the rock mass may remain dynamic well after the main instability has occurred [11].

A further complication is that failure does not always coincide with the instantaneous position of the excavation face. Time-delayed spalling has been observed days or months after excavation, and delayed rockbursts may occur after a period of apparently stable behaviour [2, 7]. Such observations imply that the rock mass response is controlled not only by the current stress state but also by loading history, accumulated damage, frictional evolution along discontinuities and time-dependent deformation. They therefore motivate a modelling framework in which excavation is represented as a transient process with internal memory and delayed response.

1.2 Current modelling approaches and research gap

The mechanical response of the ground surrounding TBM-excavated tunnels has been studied using analytical solutions, continuum numerical methods, discontinuum formulations and hybrid approaches. Finite element and finite difference models are routinely employed to calculate excavation-induced stress redistribution, deformation, plastic-zone development and support loading. These methods can incorporate advanced constitutive relationships and staged excavation, and they remain central to tunnel design. Three-dimensional analyses have also been used to estimate excavation-

damage zones and spalling susceptibility as functions of tunnel diameter, depth and the ratio between horizontal and vertical stresses [1].

Where structural discontinuities govern behaviour, discontinuum methods provide a more explicit representation of block interaction, joint opening, sliding and fracture propagation. Discrete-element and particle-based models have been applied to brittle spalling and structurally controlled failure, while coupled continuum-discontinuum methods have been developed to combine computational efficiency with explicit simulation of fractures and interfaces. For open TBM excavation in stratified rock, a coupled FDM-DEM model reproduced progressive tensile and shear fracturing in both intact blocks and bedding planes, as well as the growth of the loosened zone and interaction between the rock mass and the shield [3]. Such methods are particularly valuable for resolving the spatial geometry of damage and the mechanical role of individual discontinuities.

Monitoring-based research provides a complementary description of excavation response. Continuous microseismic systems have been used to relate event number, energy, source location, b-value and velocity-field changes to TBM activity and surrounding-rock stability [9]. Studies from deep tunnel projects have identified characteristic microseismic sequences associated with immediate rockbursts, spatial clustering near lithological interfaces, and changes in activity caused by structural planes or interaction between adjacent tunnels [4, 6]. These observations show that excavation-induced damage is not a single event but an evolving sequence involving nucleation, interaction and localization of fractures.

Despite these advances, most engineering analyses remain primarily concerned with the spatial distribution of stress, displacement and damage at selected excavation stages. Time dependence can be represented through viscoelastic, viscoplastic, creep or coupled hydro-mechanical constitutive laws, and fully dynamic numerical models are available, but systematic exploration of long-term temporal regimes is often computationally demanding. In particular, delayed activation, repeated stick-slip events, cumulative degradation and transitions between stable, periodic, intermittent and irregular responses are rarely treated as the central subject of the model.

This gap does not imply that continuum or discontinuum methods are inadequate. Rather, it identifies a complementary modelling need. Detailed numerical models answer where stresses and fractures develop in a specific geometry; a reduced nonlinear dynamic model can investigate how a system evolves through time, which combinations of mechanisms generate delayed instability, and how qualitative response regimes change as control parameters vary. The present work adopts the latter perspective while retaining a physical connection to excavation-induced stress transfer and discontinuity-controlled deformation.

1.3 A dynamical-systems perspective on TBM excavation

The advance of a TBM face may be interpreted as a moving source of mechanical perturbation. As the face approaches a discontinuity or a structurally defined rock block, the local normal and shear stresses evolve; after the face passes, unloading, support installation and redistribution through the surrounding rock continue to modify the mechanical state. The forcing is therefore both spatially localized and time dependent. Its effect depends on excavation velocity, distance from the face, in situ stress, stiffness of the surrounding medium, discontinuity orientation and frictional resistance.

Within a dynamical-systems formulation, a limited number of state variables can be used to represent the dominant modes of this response. Block displacement and velocity describe the fast mechanical subsystem, while an internal variable represents the slower evolution of damage, frictional weakening or structural degradation. This separation between fast motion and slow state evolution is consistent with field observations in which many small fracture events accumulate before a more energetic instability, or in which a disturbed zone remains apparently quiet before delayed spalling or slip occurs [2, 11].

Memory is introduced because the resistance of a discontinuity or damaged rock bridge is not determined solely by the current displacement and velocity. Previous loading cycles may polish joint asperities, degrade rock bridges, redistribute contact forces and alter local pore pressure. Consequently, the same excavation-induced stress perturbation can generate different responses depending on the previous evolution of the system. In mathematical terms, an internal memory variable allows the effective frictional or strength response to evolve as damage is accumulated and partially recovered.

Delay provides a distinct but related mechanism. Stress transfer across a heterogeneous rock mass is not equivalent to an instantaneous rigid interaction, and macroscopic failure may require finite time for subcritical crack growth, creep, fracture coalescence or progressive mobilization of a discontinuity. A delay term can therefore represent the lag between a change caused by face advance and the resulting mechanical response of another part of the system. Earlier delayed spring-block models developed for excavation-triggered fault reactivation demonstrated that even a simple frictional oscillator can exhibit equilibrium, periodic, quasi-periodic and chaotic regimes when delayed interaction is introduced [5]. The present study transfers this general concept from mining-induced fault slip to the moving, localized perturbation associated with TBM excavation.

Finally, stochastic forcing is required because natural rock masses are heterogeneous and only partially characterized. Variations in joint persistence, infill, roughness, intact-rock strength, groundwater conditions and local stress create fluctuations that cannot be represented deterministically at the scale of a reduced model. Noise is not treated merely as measurement error; it represents unresolved geological and operational variability that may trigger transitions when the system is close to instability.

Together, nonlinearity, memory, delay and stochasticity provide a compact framework for investigating several recurring patterns observed during TBM excavation: stable passage of the face, isolated microseismic events, clustered activity, delayed slip, progressive spalling and irregular event sequences. The model is not intended to replace project-specific stress analysis. Its purpose is to identify mechanisms and parameter combinations that can generate these temporal patterns and to provide hypotheses that can subsequently be tested against monitoring data or higher-fidelity simulations.

1.4 Objectives and contributions of this study

The objective of this study is to develop a reduced nonlinear dynamic model for the response of a jointed rock mass to TBM-driven tunnel excavation. The advancing face is represented as a moving source of stress perturbation acting on mechanically interacting rock blocks or structural elements. Their fast stick-slip dynamics are coupled to a slowly evolving memory variable, delayed mechanical interaction and stochastic forcing.

The study makes four principal contributions. First, it reformulates the excavation-triggered spring-block concept for a moving TBM face rather than a spatially fixed or uniformly driven underground excavation. Second, it introduces an internal memory mechanism to represent cumulative damage and the evolution of effective frictional resistance. Third, it incorporates finite interaction delay to describe lagged stress transfer and delayed activation following face passage. Fourth, it establishes a regime-based interpretation in which stable response, intermittent slip, clustered events and complex irregular behaviour are examined within one mathematical framework.

The intended outputs are therefore not detailed predictions of stress at every point around a particular tunnel. Instead, the analysis seeks to determine how excavation velocity, coupling stiffness, frictional parameters, memory rate, delay and stochastic intensity influence the timing and organization of instability. The resulting response measures may be interpreted in relation to displacement bursts, slip events, microseismic event sequences and progressive damage indicators. This makes the framework potentially useful for designing monitoring hypotheses, selecting diagnostic parameters and identifying combinations of conditions that warrant more detailed numerical or site-specific investigation.

The model is deliberately conceptual and its applicability is restricted to tunnel sections in which rock-mass discontinuities and brittle or frictional processes are mechanically relevant. Calibration against field measurements is outside the scope of the initial theoretical study, but the formulation is constructed so that TBM operational data, displacement monitoring and microseismic catalogues can be incorporated in subsequent work. In this sense, the proposed approach is complementary to continuum and discontinuum simulations: those methods resolve geometry and spatial stress redistribution, whereas the present model isolates the temporal mechanisms responsible for memory-dependent and delayed instability.

The remainder of the paper is organized as follows. Section 2 introduces the mechanical concept and mathematical formulation, including the moving-face forcing, nonlinear friction law, delay, memory evolution and stochastic terms. Section 3 describes the numerical procedure and parameter space. Section 4 presents the principal dynamic regimes and sensitivity analyses. Section 5 discusses their geomechanical interpretation, limitations and implications for TBM monitoring. Section 6 summarizes the main findings and identifies priorities for calibration and model extension.

2. Conceptual and Mathematical Model

2.1 Physical representation of the TBM-rock mass system

The proposed framework represents TBM excavation as a moving mechanical disturbance acting on a discontinuous and progressively evolving rock mass. As the excavation face advances, the initial stress field is locally redistributed, producing zones of unloading, stress concentration, fracture development, and possible activation of pre-existing discontinuities. These effects evolve continuously with the position of the excavation face and may persist after the TBM has passed the affected section.

The surrounding rock mass is idealized as a system of mechanically interacting blocks separated by joints, bedding planes, fractures, or fault surfaces. Each block represents a characteristic rock volume whose motion reflects the cumulative response of a larger discontinuity-bounded domain rather than the displacement of an individual physical fragment. The interaction between adjacent blocks is represented by elastic coupling, whereas resistance to motion is governed by a nonlinear friction law acting along structural discontinuities.

The advancing TBM face is treated as a moving source of stress perturbation. Its position is defined as

$$x_f(t) = x_{f,0} + v_f t,$$

where $x_{f,0}$ is the initial face position and v_f is the TBM advance rate. The distance between the excavation face and the i-th rock block is therefore

$$d_i(t) = X_i - x_f(t),$$

where X_i denotes the fixed spatial position associated with the block or structural discontinuity.

The excavation-induced mechanical forcing depends on this relative distance. Before the face reaches a given location, the block may experience increasing stress concentration. Near the face, the perturbation reaches its highest intensity, whereas behind the face the rock mass progressively unloads and adjusts to the newly formed excavation boundary. The resulting loading history is therefore spatially localized, time dependent, and generally asymmetric with respect to the face position.

Within this conceptual representation, localized instability is interpreted as a transition from stable or slowly evolving deformation to rapid slip along a discontinuity. Such slip events may correspond to fracture activation, local block movement, microseismic events, strainburst-type damage, or small fault-slip episodes, depending on the geological and stress conditions.

2.2 Moving excavation-induced forcing

The mechanical influence of the advancing excavation face is introduced through a spatial transfer function $G(d_i)$, which describes the variation of excavation-induced loading with distance from the face. The external forcing acting on block i is written as

$$q_i(t) = Q_i G[d_i(t)],$$

where Q_i is the characteristic amplitude of the excavation-induced perturbation.

A convenient general form of the transfer function is

$$G(d) = \begin{cases} A_f \exp\left(-\dfrac{d^2}{2L_f^2}\right), & d \geq 0, \\ A_b \exp\left(\dfrac{d}{L_b}\right), & d < 0, \end{cases}$$

where L_f and L_b are the characteristic influence lengths ahead of and behind the excavation face, respectively, while A_f and A_b control the corresponding forcing amplitudes.

This formulation allows the mechanical effect of the excavation to differ in front of and behind the TBM. Such asymmetry is physically justified because the rock mass ahead of the face remains confined, whereas the region behind the face has already been excavated, unloaded, and partially stabilized by the tunnel support system. The parameters L_f, L_b, A_f, and A_b may therefore be related to excavation diameter, in situ stress level, rock mass stiffness, support installation distance, and the operational characteristics of the TBM.

The forcing term $q_i(t)$ does not represent the detailed three-dimensional stress field around the tunnel. Instead, it provides a reduced-order description of the time-dependent mechanical disturbance experienced by a characteristic discontinuity or rock block as the excavation face approaches, passes, and moves away.

2.3 Fast mechanical subsystem

The short-term mechanical response of the rock mass is described by a system of coupled nonlinear equations. For a two-block representation, the displacement and velocity perturbations of block i are denoted by $x_i(t)$ and $y_i(t)$, respectively, where $i = 1,2$ and $j = 3 - i$.

The governing equations are

$$\dot{x}_i(t) = y_i(t),$$

$$\dot{y}_i(t) = -r_i(\chi_i)\,\Delta F_i - k_i x_i(t) + k_c\left[x_j\left(t-\tau_{ij}\right) - x_i(t)\right] + q_i(t) + \sigma_i \xi_i(t).$$

Here, k_i is the effective stiffness connecting block i to the surrounding rock mass, k_c is the coupling stiffness between adjacent blocks, and τ_{ij} is the interaction delay between them. The term $q_i(t)$ represents the excavation-induced forcing, while $\xi_i(t)$ is a stochastic process with intensity σ_i.

The term

$$k_c\left[x_j\left(t-\tau_{ij}\right) - x_i(t)\right]$$

describes delayed stress transfer between mechanically interacting rock domains. A disturbance generated in one part of the rock mass does not necessarily influence an adjacent discontinuity instantaneously. The effective delay may reflect progressive fracture propagation, redistribution of contact forces, viscoelastic relaxation, pore-pressure diffusion, or gradual mobilization of frictional resistance.

The coefficient $r_i(\chi_i)$ controls the influence of the evolving internal state on the frictional response. As damage accumulates, the resistance of a discontinuity may decrease, thereby increasing the likelihood of rapid slip.

2.4 Nonlinear friction law

The relative motion of a block along a discontinuity is governed by a nonlinear friction law. Following a reduced-order stick-slip representation, the friction force is expressed as a function of the total sliding velocity,

$$u_i = V_i + y_i,$$

where V_i is a reference loading or deformation velocity and y_i is the velocity perturbation.

The nonlinear friction function is defined as

$$F(u) = au^3 - bu^2 + cu,$$

and the incremental frictional contribution is

$$\Delta F_i = F(V_i + y_i) - F(V_i).$$

The coefficients a, b, and c control the shape of the friction-velocity relation. Depending on their values, the model can reproduce velocity-strengthening and velocity-weakening intervals, which are essential for generating transitions between stable sliding and dynamic instability.

The use of a nonlinear friction law is not intended to reproduce the complete microscale mechanics of rock joints. Instead, it represents the effective macroscopic resistance of a

discontinuity whose shear strength depends on the rate and history of relative motion. Such a formulation allows the model to produce stable equilibrium, periodic slip, intermittent activation, and irregular dynamic responses within a unified framework.

2.5 Memory and damage evolution

To represent progressive degradation and loading-history dependence, each block is assigned an internal memory variable $\chi_i(t)$. This variable describes the cumulative mechanical state of the corresponding rock domain and may be interpreted as a normalized measure of damage, joint degradation, fracture accumulation, or loss of frictional resistance.

The evolution of memory is described by

$$\dot{\chi}_i = \alpha_i \Phi_i - \beta_i \chi_i,$$

where α_i is the damage accumulation coefficient, β_i is the recovery or relaxation coefficient, and Φ_i is a measure of current mechanical activity.

A possible definition is

$$\Phi_i = y_i^2 + \lambda_i \left[x_j\left(t - \tau_{ij}\right) - x_i(t)\right]^2 + \eta_i q_i^2(t),$$

where the first term represents slip-related activity, the second describes deformation associated with interaction between adjacent blocks, and the third accounts for damage caused directly by excavation-induced loading.

The memory variable therefore increases during periods of intense mechanical activity and gradually decreases when the system remains weakly disturbed. The relaxation term should not necessarily be interpreted as complete healing of the rock mass. It represents the partial recovery of frictional contact, stress relaxation, stabilization by support, or the decay of transient damage-related effects.

The influence of memory on the frictional resistance is introduced through

$$r_i(\chi_i) = r_{0i} \exp(-\gamma_i \chi_i),$$

where r_{0i} is the initial friction scaling coefficient and γ_i controls the sensitivity of the discontinuity to accumulated damage.

As χ_i increases, the effective frictional resistance decreases. Consequently, a rock domain that has experienced repeated loading, fracture development, or previous slip becomes more susceptible to subsequent activation. This formulation allows the system to retain information about its loading history and to produce different responses under identical instantaneous excavation conditions.

2.6 Delayed response

Delayed response is introduced through the displacement term $x_j(t-\tau_{ij})$. The parameter τ_{ij} represents the finite time between a mechanical disturbance in one part of the rock mass and its effective influence on another.

In the context of TBM excavation, this delay may include several physical contributions:

$$\tau_{ij} = \tau_\sigma + \tau_f + \tau_p + \tau_s,$$

where τ_σ is the characteristic stress-transfer time, τ_f is associated with progressive fracture development, τ_p represents pore-pressure redistribution, and τ_s reflects the delayed influence of support installation or annular grouting.

The individual terms are not necessarily resolved separately in the reduced-order model. Instead, τ_{ij} is treated as an effective parameter controlling the time lag between coupled rock-mass responses.

When $\tau_{ij} = 0$, the blocks interact instantaneously. For finite values of τ_{ij}, the current motion of one block depends on the previous state of another. Such delayed interaction may destabilize an otherwise stable system and generate oscillatory, intermittent, or irregular motion.

2.7 Stochastic heterogeneity

Natural rock masses are spatially heterogeneous and contain unavoidable uncertainty in fracture geometry, strength, stiffness, groundwater conditions, and in situ stress. In addition, TBM operational parameters such as penetration rate, thrust, torque, and face pressure fluctuate during excavation.

These effects are represented through the stochastic term

$$\sigma_i \xi_i(t),$$

where $\xi_i(t)$ is assumed to be a zero-mean stochastic process satisfying

$$\langle \xi_i(t) \rangle = 0,$$

$$\langle \xi_i(t)\xi_j(t') \rangle = \delta_{ij}\delta(t-t').$$

The parameter σ_i controls the intensity of stochastic fluctuations.

The purpose of this term is not to treat all geological variability as random noise. Rather, it represents unresolved heterogeneity at scales smaller than those explicitly included in the model. It also allows the investigation of noise-induced slip, variability in event timing, and transitions between stable and unstable regimes.

2.8 Complete coupled model

The resulting two-block TBM-rock mass model is

$$\dot{x}_i = y_i,$$

$$\dot{y}_i = -r_{0i}\exp(-\gamma_i\chi_i)[F(V_i + y_i) - F(V_i)] - k_i x_i + k_c\left[x_j\left(t - \tau_{ij}\right) - x_i(t)\right] + Q_i G[d_i(t)] + \sigma_i\xi_i(t),$$

$$\dot{\chi}_i = \alpha_i\left[y_i^2 + \lambda_i\left(x_j\left(t - \tau_{ij}\right) - x_i(t)\right)^2 + \eta_i Q_i^2 G^2[d_i(t)]\right] - \beta_i\chi_i,$$

with

$$d_i(t) = X_i - x_{f,0} - v_f t,$$

and

$$F(u) = au^3 - bu^2 + cu.$$

This system combines a fast mechanical subsystem, a slow internal memory subsystem, delayed coupling, moving excavation-induced forcing, and stochastic heterogeneity.

The model is intentionally formulated as a reduced-order representation. It does not resolve the complete geometry of the tunnel, the detailed cutting process at the TBM face, or the full three-dimensional stress field. Instead, it isolates the principal mechanisms considered responsible for the temporal complexity of excavation-induced instability.

2.9 Dimensionless formulation

For numerical analysis, the governing equations may be expressed in dimensionless form. Let

$$x_i = x_c\bar{x}_i, \qquad t = t_c\bar{t}, \qquad y_i = \frac{x_c}{t_c}\bar{y}_i,$$

where x_c and t_c are characteristic displacement and time scales.

The characteristic time may be defined as

$$t_c = \sqrt{\frac{m}{k_r}},$$

where m is the effective block mass and k_r is a reference stiffness.

After substitution and omission of the overbars, the dimensionless system becomes

$$\dot{x}_i = y_i,$$

$$\dot{y}_i = -\rho_i(\chi_i)\Delta f_i - \kappa_i x_i + \kappa_c\left[x_j\left(t - \theta_{ij}\right) - x_i(t)\right] + p_i g[d_i(t)] + s_i\xi_i(t),$$

$$\dot{\chi}_i = A_i\left[y_i^2 + \Lambda_i\left(x_j\left(t - \theta_{ij}\right) - x_i(t)\right)^2 + H_i p_i^2 g^2[d_i(t)]\right] - B_i\chi_i.$$

The dimensionless parameters describe the relative importance of stiffness, friction, memory, delay, excavation forcing, and stochastic heterogeneity. This formulation facilitates systematic parameter studies and the identification of dynamic regimes that are independent of a particular system of physical units.

2.10 Model outputs and physical interpretation

The principal state variables of the model are displacement x_i, velocity y_i, and memory χ_i. Dynamic slip events are identified when the block velocity exceeds a prescribed threshold,

$$|y_i(t)| > y_{\mathrm{cr}}.$$

The event duration is defined as the interval during which this condition remains satisfied. A dimensionless event intensity may be estimated as

$$E_i = \int_{t_a}^{t_b} y_i^2\,(t)\,dt,$$

where t_a and t_b denote the beginning and end of an event.

In engineering terms:

1. small-amplitude stable motion represents gradual deformation and stress adjustment;
2. isolated velocity peaks represent local fracture activation or low-energy microseismic events;
3. repeated periodic peaks represent recurrent stick-slip activation;
4. clustered peaks represent progressive fracture interaction or event sequences;
5. large irregular peaks indicate complex unstable behaviour and elevated susceptibility to localized dynamic failure;
6. persistent growth of χ_i indicates cumulative degradation and increasing sensitivity to subsequent excavation-induced disturbance.

The model outputs should therefore be interpreted as indicators of dynamic regime and instability potential rather than direct predictions of earthquake magnitude, tunnel convergence, or TBM operational demand. Quantitative project-specific prediction would require calibration against site investigation data, stress measurements, TBM operational records, and microseismic monitoring.

3. Numerical Methodology and Parameter Selection

3.1 Numerical integration strategy

The governing equations form a nonlinear stochastic delay differential system with coupled fast and slow variables. The presence of delayed interaction terms requires the numerical procedure to retain the displacement history of each block over the interval required by the prescribed delays.

The deterministic part of the system is integrated using a fixed-step fourth-order Runge-Kutta scheme, while the stochastic contribution is introduced through independent Gaussian increments. For the i-th block, the numerical update is based on the system

$$\dot{x}_i = y_i,$$

$$\dot{y}_i = -\rho_i(\chi_i)\Delta f_i - \kappa_i x_i + \kappa_c\left[x_j\left(t-\theta_{ij}\right) - x_i(t)\right] + p_i g[d_i(t)] + s_i\xi_i(t),$$

$$\dot{\chi}_i = A_i\left[y_i^2 + \Lambda_i\left(x_j\left(t-\theta_{ij}\right) - x_i(t)\right)^2 + H_i p_i^2 g^2[d_i(t)]\right] - B_i\chi_i.$$

For stochastic simulations, the white-noise term is approximated over each time interval Δt by

$$s_i\xi_i(t)\,dt \approx s_i\sqrt{\Delta t}\,Z_i,$$

where Z_i is a standard normally distributed random variable.

The delayed displacement $x_j\left(t-\theta_{ij}\right)$ is evaluated from the stored numerical history. Linear interpolation is used whenever the delayed time does not coincide exactly with a previously computed time step.

A constant history function is prescribed before the beginning of the simulation,

$$x_i(t) = x_{i,0}, \qquad y_i(t) = 0, \qquad \chi_i(t) = \chi_{i,0}, \qquad t \in [-\theta_{\max}, 0],$$

where $\theta_{\max}$ denotes the largest delay considered in the analysis.

The time-step size is selected through a convergence analysis. Numerical solutions are compared for progressively smaller values of Δt, and the adopted step is required to preserve the event sequence, peak velocities, and long-term dynamic regime.

3.2 Simulation domain and initial configuration

The model represents two characteristic rock domains located along the TBM excavation path. Their fixed spatial coordinates are denoted by X_1 and X_2, with

$$X_2 > X_1.$$

The dimensionless face position is defined as

$$x_f(t) = x_{f,0} + v_f t.$$

The simulation begins with the excavation face sufficiently far from both blocks so that the initial forcing is negligible,

$$g[d_i(0)] \approx 0.$$

The total simulation duration is selected so that the face passes both modelled domains and advances sufficiently far beyond them to capture delayed post-passage responses. Accordingly,

$$t_{\mathrm{end}} > \frac{X_2 - x_{f,0}}{v_f} + \theta_{\max} + t_r,$$

where t_r is an additional relaxation period.

The first block may be interpreted as a rock domain closer to the initial excavation position, while the second represents a neighbouring discontinuity-controlled domain activated later by the advancing face and by mechanical interaction with the first block.

Unless otherwise stated, both blocks are initialized close to mechanical equilibrium with small displacement perturbations. The use of nonzero perturbations prevents the numerical solution from remaining artificially constrained to a perfectly symmetric state.

3.3 Baseline parameter set

A dimensionless baseline parameter set is introduced to represent a moderately coupled and weakly heterogeneous rock mass subjected to a moving excavation disturbance. The baseline values are selected to produce stable behaviour in the absence of excavation forcing while allowing transitions to slip instability when memory, delay, or forcing intensity increases.

The reference parameter set is defined as

$$a = 3.2, \qquad b = 7.2, \qquad c = 4.8,$$

$$V_1 = V_2 = 1.0,$$

$$\kappa_1 = \kappa_2 = 1.0, \qquad \kappa_c = 0.25,$$

$$\rho_{01} = \rho_{02} = 1.0, \qquad \gamma_1 = \gamma_2 = 0.8,$$

$$A_1 = A_2 = 0.02, \qquad B_1 = B_2 = 0.005,$$

$$\Lambda_1 = \Lambda_2 = 0.5, \qquad H_1 = H_2 = 0.2,$$

$$p_1 = p_2 = 0.6, \qquad s_1 = s_2 = 0.01,$$

$$\theta_{12} = \theta_{21} = 0.5.$$

The spatial positions are prescribed as

$$X_1 = 20, \qquad X_2 = 30,$$

while the excavation face starts at

$$x_{f,0} = 0.$$

The reference advance rate is

$$v_f = 0.1.$$

These values are not intended to represent a specific tunnel project. They define a reference dynamic system from which the individual effects of stiffness, memory, delay, forcing, advance rate, and stochasticity can be investigated systematically.

3.4 Excavation influence function

The dimensionless forcing function is defined separately ahead of and behind the excavation face:

$$g(d) = \begin{cases} \exp\left(-\dfrac{d^2}{2L_f^2}\right), & d \geq 0, \\ R_b \exp\left(\dfrac{d}{L_b}\right), & d < 0. \end{cases}$$

The baseline values are

$$L_f = 5, \qquad L_b = 8, \qquad R_b = 0.6.$$

The larger post-passage influence length reflects the possibility that unloading, fracture evolution, and support interaction continue after the face has passed the considered rock domain.

The face reaches the i-th block at the nominal passage time

$$t_{f,i} = \frac{X_i - x_{f,0}}{v_f}.$$

This time provides a reference for analysing whether a slip event occurs before, during, or after the local passage of the TBM face.

The event delay relative to face passage is defined as

$$\Delta t_{e,i} = t_{e,i} - t_{f,i},$$

where $t_{e,i}$ is the onset time of a detected dynamic event.

Negative values of $\Delta t_{e,i}$ indicate activation ahead of the face, while positive values indicate delayed response behind the face.

3.5 Parameter ranges

The model response is investigated over parameter ranges selected to cover stable, transitional, and unstable behaviour.

The TBM advance rate is varied within

$$0.02 \leq v_f \leq 0.30.$$

The excavation forcing amplitude is varied within

$$0 \leq p_i \leq 1.5.$$

The block coupling stiffness is investigated over

$$0 \leq \kappa_c \leq 1.0.$$

The interaction delay is varied within

$$0 \leq \theta_{ij} \leq 5.0.$$

The memory accumulation coefficient is examined over

$$0 \leq A_i \leq 0.10,$$

while the relaxation coefficient is varied within

$$0.001 \leq B_i \leq 0.05.$$

The memory sensitivity of friction is varied over

$$0 \leq \gamma_i \leq 2.0.$$

Finally, the stochastic intensity is investigated within

$$0 \leq s_i \leq 0.10.$$

The selected ranges are broad enough to identify qualitative changes in the system dynamics without assigning direct project-specific physical units to the dimensionless variables.

3.6 Simulation programme

The numerical analysis is organized into a sequence of simulation groups designed to isolate the influence of individual mechanisms.

3.6.1 Reference excavation response

The baseline simulation is first performed to characterize the response of the coupled system to the passage of the excavation face. The analysis includes:

7. displacement histories;
8. block velocities;
9. memory evolution;
10. excavation forcing histories;
11. event timing relative to face passage;
12. phase-plane trajectories.

This simulation defines the reference behaviour against which subsequent parameter changes are compared.

3.6.2 Influence of TBM advance rate

The advance rate v_f controls both the duration and the rate of excavation-induced loading. At low advance rates, a rock domain remains exposed to the forcing zone for a longer period, allowing damage and memory to accumulate gradually. At higher advance rates, the disturbance is shorter but changes more rapidly.

The simulations therefore examine whether changes in v_f produce:

1. suppression or amplification of peak velocity;
2. changes in event delay;
3. changes in the number of slip events;
4. transition from gradual deformation to dynamic activation;
5. different levels of accumulated memory.

3.6.3 Influence of forcing intensity

The amplitude p_i represents the magnitude of the local excavation-induced mechanical perturbation. It may be interpreted as a reduced-order indicator of stress level, excavation diameter, geological confinement, or concentration of loading around the face.

The forcing amplitude is increased gradually to identify threshold values separating stable passage from dynamic slip.

3.6.4 Influence of delayed coupling

The delay parameter θ_{ij} is varied to evaluate the role of delayed stress transfer between the two rock domains.

The analysis focuses on whether increasing delay causes:

1. destabilization of steady response;
2. oscillatory behaviour;
3. repeated slip;
4. event clustering;
5. irregular or chaotic dynamics.

The results are compared with the zero-delay system to isolate the contribution of delayed interaction.

3.6.5 Influence of memory

The parameters A_i, B_i, and γ_i control damage accumulation, relaxation, and the effect of memory on frictional resistance.

Simulations are performed for:

1. no-memory conditions;
2. weak memory;
3. rapidly accumulating memory;
4. slowly relaxing memory;
5. high friction sensitivity to damage.

The comparison establishes whether delayed instability can emerge even after the direct excavation forcing has begun to decay.

3.6.6 Influence of stochastic heterogeneity

For nonzero s_i, each parameter combination is simulated over multiple stochastic realizations.

The ensemble analysis evaluates:

1. variability of event onset time;
2. probability of slip occurrence;
3. distribution of peak velocities;
4. event-energy variability;
5. sensitivity of nominally stable regimes to noise.

At least N_r independent realizations are used for each stochastic parameter set, where N_r should be sufficiently large to obtain stable ensemble statistics.

3.7 Event-detection procedure

Dynamic events are identified from the velocity time series. An event begins when

$$|y_i(t)| \geq y_{\mathrm{on}},$$

and ends when

$$|y_i(t)| < y_{\mathrm{off}},$$

where

$$y_{\mathrm{off}} < y_{\mathrm{on}}.$$

The use of separate onset and termination thresholds prevents a single event from being divided into multiple events due to small fluctuations around the detection threshold.

The baseline thresholds are selected as

$$y_{\text{on}} = 0.10, \qquad y_{\text{off}} = 0.05.$$

For each event, the following quantities are calculated:

$$t_e = \text{event onset time},$$

$$T_e = t_b - t_a,$$

$$y_{\max} = \max_{t\in[t_a,t_b]} |y_i(t)|,$$

$$D_e = \int_{t_a}^{t_b} |y_i(t)|\ dt,$$

$$E_e = \int_{t_a}^{t_b} y_i^2\,(t)\,dt.$$

Here, T_e is event duration, D_e is a displacement-related event measure, and E_e is a dimensionless kinetic-energy indicator.

An interaction event is recorded when slip in one block is followed by activation of the second block within a prescribed coupling window.

3.8 Dynamic regime classification

The system response is classified using time histories, phase-space trajectories, spectral characteristics, event statistics, and sensitivity to initial conditions.

The principal regimes are defined as follows.

Stable response
The velocities decay toward zero or remain below the event threshold, while memory remains bounded at a low level.

Single excavation-induced event
A single dominant velocity peak occurs during or shortly after the passage of the excavation face, followed by relaxation toward a stable state.

Intermittent slip
Several isolated events occur, separated by intervals of weak motion.

Periodic response
Slip events recur with approximately constant time intervals and comparable amplitudes.

Quasiperiodic response
The response contains two or more incommensurate characteristic frequencies and exhibits modulated event amplitudes.

Clustered activity
Events occur in groups separated by relatively long inactive intervals. Such behaviour may represent progressive interaction between discontinuities or delayed activation of neighbouring rock domains.

Irregular or chaotic response
The motion is aperiodic, strongly sensitive to initial conditions, and associated with a broadband frequency spectrum or a positive largest Lyapunov exponent.

This classification is used as a dynamical interpretation of the model response and not as a direct classification of field-scale seismic hazard.

3.9 Bifurcation analysis

To identify transitions between dynamic regimes, one control parameter is varied while the remaining parameters are held constant.

After removal of the initial transient response, local maxima of block velocity are extracted and plotted against the selected control parameter. The resulting bifurcation diagrams are constructed for

$$v_f, \qquad p_i, \qquad \theta_{ij}, \qquad A_i, \qquad \gamma_i, \qquad \kappa_c.$$

The bifurcation analysis is intended to determine whether gradual changes in excavation or rock-mass parameters produce abrupt transitions between stable, periodic, intermittent, and irregular responses.

Because the forcing is transient rather than permanently stationary, bifurcation diagrams may also be constructed from event-based measures, including

$$y_{\max}, \qquad N_e, \qquad E_{\mathrm{tot}}, \qquad \Delta t_e,$$

where N_e is the number of detected events and

$$E_{\mathrm{tot}} = \sum_{e=1}^{N_e} E_e.$$

3.10 Spectral and phase-space analysis

The frequency content of the dynamic response is examined using the power spectral density of the block velocity.

Periodic solutions are expected to produce discrete spectral peaks, quasiperiodic solutions multiple incommensurate peaks, and irregular solutions broadband spectra.

Phase portraits are constructed in the planes

$$(x_i, y_i),$$

$$(y_i, \chi_i),$$

and

$$(x_1, x_2).$$

These representations provide insight into the interaction between fast mechanical response and slow damage evolution.

The delayed coupling may also be analysed using reconstructed phase spaces based on time-lagged coordinates.

3.11 Lyapunov analysis

Where irregular behaviour is observed, the largest Lyapunov exponent is estimated to distinguish deterministic chaos from stochastic variability.

For deterministic simulations with

$$s_i = 0,$$

two nearby trajectories are initialized with an initial separation δ_0. Their divergence is monitored as

$$\delta(t) \approx \delta_0 e^{\lambda_{\max} t}.$$

The largest Lyapunov exponent is estimated from the average exponential divergence rate.

A positive value,

$$\lambda_{\max} > 0,$$

indicates sensitivity to initial conditions and supports the interpretation of chaotic dynamics.

For stochastic simulations, Lyapunov analysis is treated with caution because trajectory divergence may be produced by independent noise realizations. In such cases, identical stochastic forcing must be applied to neighbouring trajectories.

3.12 Sensitivity analysis

The relative influence of the governing parameters is evaluated using both one-at-a-time and global sensitivity procedures.

The local sensitivity of an output quantity R to parameter p is estimated as

$$S_p = \frac{p}{R}\frac{\partial R}{\partial p}.$$

The principal outputs considered are:

1. maximum velocity;
2. total event number;

3. cumulative event energy;
4. maximum memory;
5. first-event delay;
6. probability of activation of the second block.

For a broader assessment, Latin hypercube sampling may be used to generate parameter combinations over the defined ranges. Rank correlation coefficients or variance-based indices may then be calculated to identify the parameters that exert the strongest control on the dynamic response.

3.13 Numerical verification

The numerical implementation is verified through several limiting cases.

First, when

$$p_i = 0, \qquad s_i = 0,$$

the system must reproduce the unforced mechanical response.

Second, when

$$A_i = 0,$$

the memory variable must not influence the mechanical subsystem.

Third, when

$$\theta_{ij} = 0,$$

the model must reduce to an instantaneously coupled system.

Fourth, when

$$\kappa_c = 0,$$

the two blocks must evolve independently except for their common exposure to the moving excavation disturbance.

Finally, repeated simulations with decreasing Δt are used to demonstrate time-step convergence.

These verification cases ensure that the numerical response follows directly from the mechanisms introduced in the mathematical formulation.

3.14 Interpretation of parameter studies

The numerical results are interpreted primarily in terms of qualitative mechanisms rather than direct site-specific prediction.

The principal questions addressed are:

1. Under which conditions does the passage of the excavation face produce stable deformation rather than dynamic slip?
2. Can memory generate delayed events after the direct forcing has decayed?
3. Does delayed coupling promote interaction and clustering between neighbouring discontinuities?
4. How does the TBM advance rate affect event timing and intensity?
5. Can stochastic heterogeneity trigger slip in a system that is stable under deterministic conditions?
6. Which combinations of parameters produce periodic, intermittent, or irregular excavation-induced responses?

The answers to these questions form the basis for the engineering interpretation presented in the subsequent sections.

4. Numerical Results and Dynamic Regimes

Interpreted numerical response, critical transitions, and engineering meaning

4.1 Baseline stable response (B0)

The deterministic B0 simulation was performed using the baseline parameter set defined in Section 3, with p = 0.75, v_f = 0.10, interaction delay θ = 0.50, and zero stochastic forcing. The excavation face reached the first and second model domains at dimensionless times t_f,1 = 200 and t_f,2 = 280, respectively.

$$t_\{f,1\} = 200, \quad t_\{f,2\} = 280$$

B0 remained below the prescribed event threshold |y_i| ≥ 0.10. The maximum velocities were 0.013866 and 0.015065, occurring approximately 2.81 time units after local face passage. The response is therefore classified as a stable excavation-induced adjustment with a small but measurable post-passage lag.

The stable response is not mechanically trivial. The passage of the face produces a clear transient displacement and a delayed velocity maximum in each domain, but the available excitation is dissipated before the velocity-weakening branch can sustain repeated motion. The approximately equal post-passage delay of the two velocity maxima indicates that this lag is controlled mainly by the local shape of the moving forcing function, rather than by progressive inter-domain transfer.

Memory nevertheless continues to evolve after the strongest mechanical response. In B0, however, the associated reduction in the friction scale remains modest, so the slow subsystem records the excavation history without converting it into dynamic instability. B0

therefore provides the necessary control case: excavation-induced deformation and memory accumulation can occur without threshold-exceeding slip.

Quantity	Block 1	Block 2
Maximum absolute velocity	0.013866	0.015065
Time of maximum velocity	202.81	282.81
Delay from face passage	2.81	2.81
Maximum absolute displacement	0.65714	0.67801
Maximum memory	0.15591	0.16425
Minimum friction scale ρ	0.91070	0.90615
Events above threshold	0	0

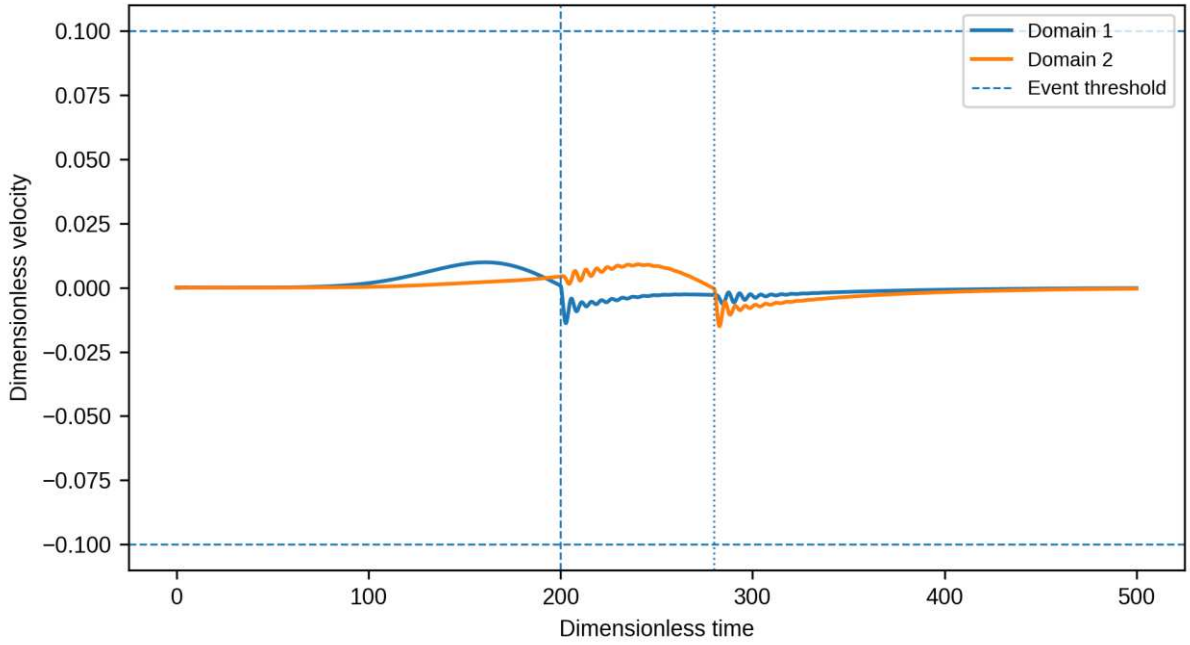


Fig. 1 Velocity histories for the stable B0 reference case

4.2 Near-critical delayed instability (B1)

B1 was defined by increasing only the excavation forcing amplitude from p = 0.75 to p = 3.15. All other parameters remained identical to B0. This single-parameter modification transformed the response from stable adjustment into a delayed transient cluster of stick–slip events.

$$B1: p_1 = p_2 = 3.15$$

The second domain became active first, at t = 382.805, corresponding to a delay of 102.805 after local face passage. It generated eleven events. The first domain became active at t = 401.670, 201.670 time units after face passage, and generated four events.

The reversal of the spatial passage order demonstrates that instability timing is governed by memory evolution and delayed coupling, rather than by face position alone.

The delayed onset is the defining feature of B1. At the time of first activation, the face has already moved well beyond both modelled locations and the direct forcing has decayed substantially. The events must therefore be interpreted as the release of a mechanically weakened state created during earlier face passage, rather than as an instantaneous response to the current face position.

The reversed activation order is also physically important. The downstream domain is exposed to its own loading history while simultaneously receiving delayed deformation from the upstream domain. This combined history produces a lower effective resistance and allows the downstream block to enter the event regime first. Thus, spatial order along the tunnel does not necessarily determine temporal order of failure.

The repeated peaks in the velocity record form a transient cluster rather than a permanent periodic attractor. Their amplitude remains bounded and the activity eventually decays as the excavation disturbance moves away and memory relaxes. B1 is therefore interpreted as near-critical clustered stick-slip, not as sustained seismic cycling.

Quantity	**Block 1**	**Block 2**
Maximum absolute velocity	0.101036	0.107531
Time of maximum velocity	412.49	409.85
Detected events	4	11
First-event onset	401.670	382.805
Delay from face passage	201.670	102.805
Maximum memory	2.7524	2.8994
Minimum friction scale ρ	0.1918	0.1756

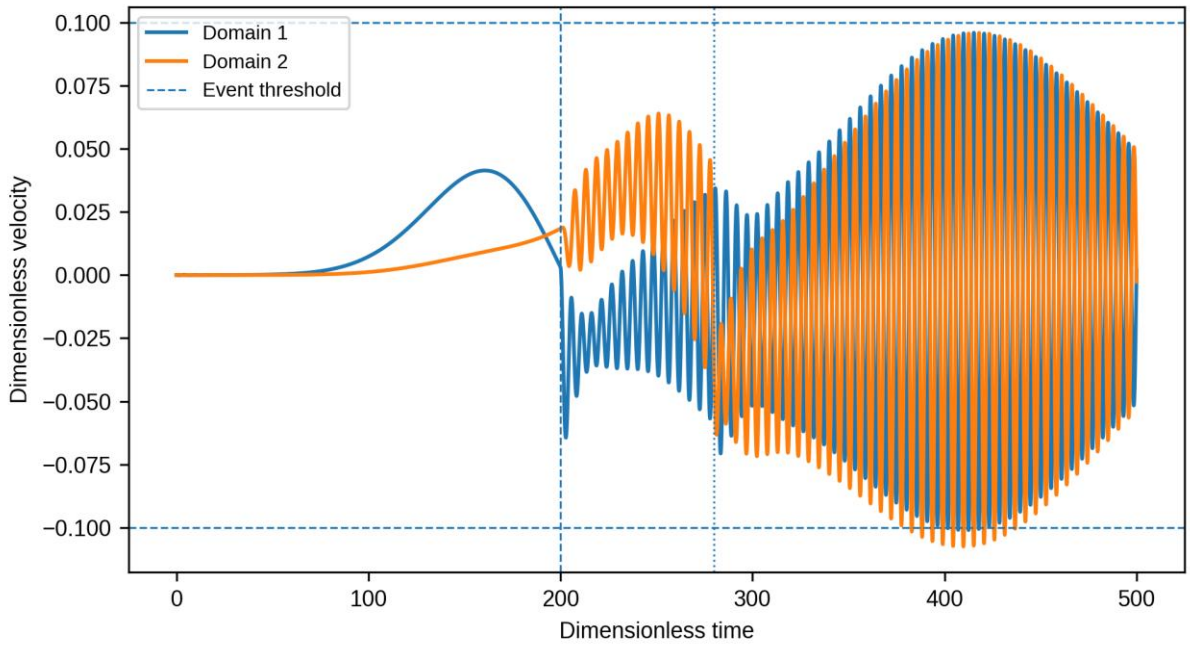


Fig. 2 B1 velocity histories and the event threshold

4.3 Critical excavation-forcing transition

A narrow sweep of p identified a sharp transition from stable response through selective activation of the second domain to coupled clustered activity. No threshold-exceeding events were detected for $p \leq 3.13$. At $p = 3.14$ only the second domain became active, whereas at $p = 3.15$ both domains crossed the event threshold.

The forcing sweep separates three mechanically distinct responses. Below the first threshold, the excavation perturbation changes displacement and memory but cannot produce threshold-exceeding motion. In the selective interval, only the downstream domain reaches the dynamic criterion. A further small increase in forcing activates both domains and rapidly increases the number and cumulative intensity of events.

The transition is considerably sharper in event count than in peak velocity. This distinction matters because a modest change in the largest recorded velocity can correspond to a large change in the duration and repetition of activity. Peak amplitude alone would therefore underestimate the qualitative change in system behaviour near the critical forcing level.

Because p is dimensionless, the threshold should not be interpreted as a universal stress magnitude for TBM projects. It defines the critical excitation of the present reduced-order system. Project-specific use would require calibration of p against numerical stress changes, machine loads, or measured ground response.

p	max $\lvert y_1 \rvert$	max $\lvert y_2 \rvert$	Events 1	Events 2	Regime
3.10	0.0756	0.0812	0	0	Stable

3.12	0.0852	0.0911	0	0	Stable
3.13	0.0903	0.0964	0	0	Stable
3.14	0.0956	0.1019	0	6	Selective
3.15	0.1010	0.1075	4	11	Coupled
3.16	0.1066	0.1133	15	19	Coupled
3.18	0.1180	0.1253	29	32	Coupled
3.20	0.1299	0.1377	37	40	Coupled

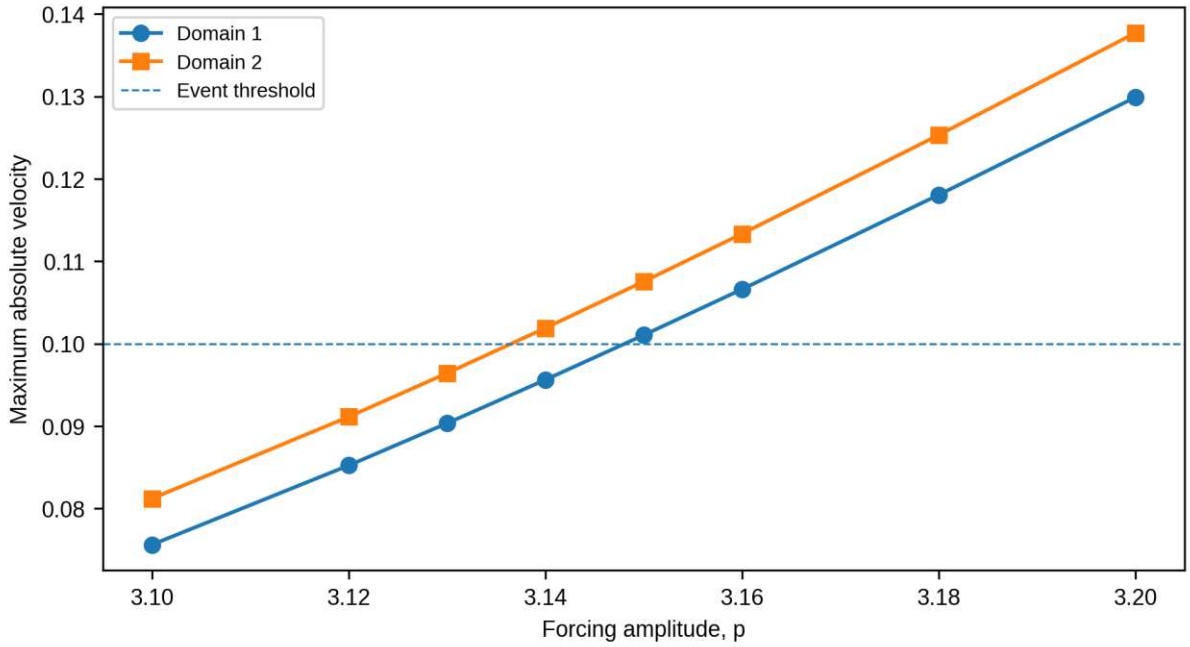


Fig. 3 Maximum velocity across the critical forcing interval

4.4 Influence of TBM advance rate

The influence of v_f was strongly non-monotonic. Low advance rates promoted memory-dominated degradation because each domain remained within the excavation influence zone for a long time. Intermediate rates produced a narrow stabilization window. Higher rates generated a second, impulsive instability branch associated with rapid near-face loading.

At low advance rates, the moving disturbance acts for a long time at each location. The resulting instability is therefore memory dominated: damage-related state variables accumulate, friction remains weakened for a prolonged interval, and repeated events can continue after local face passage. Increasing the advance rate initially shortens exposure and suppresses this mechanism.

At high advance rates, instability reappears for a different reason. The disturbance varies rapidly and the mechanical subsystem responds more impulsively, even though the

maximum accumulated memory is lower. The low- and high-rate branches are therefore not equivalent: one is controlled by prolonged weakening, while the other is controlled by rapid excitation.

v_f	max $\|y_1\|$	max $\|y_2\|$	Events 1	Events 2	Regime
0.04	0.687	0.784	131	131	Memory-dominated
0.06	0.441	0.483	104	104	Memory-dominated
0.08	0.270	0.290	87	87	Memory-dominated
0.10	0.101	0.108	4	11	Delayed coupled
0.12	0.075	0.112	0	1	Selective
0.15	0.090	0.084	0	0	Stable
0.18	0.104	0.124	1	2	Coupled
0.20	0.113	0.148	1	4	Impulsive
0.25	0.133	0.155	2	5	Impulsive

A local sweep established a numerically confirmed stable interval of 0.148 ≤ v_f ≤ 0.152. Instability immediately outside this interval was restricted to the second domain. The advance-rate response therefore has a U-shaped structure: instability at low rates, stabilization at intermediate rates, and renewed instability at high rates.

The stable interval is narrow and is controlled by the downstream domain. Across the local sweep, the upstream block remains below the event threshold, whereas the downstream response crosses it on both sides of the stable window. This result identifies the second domain as the more sensitive indicator of changes in advance rate.

The existence of a stability window should not be interpreted as a direct operational recommendation for a dimensional TBM advance rate. The value is model dependent. Its significance is conceptual: an intermediate rate may avoid both prolonged exposure and impulsive loading, whereas either slower or faster advance can promote instability through different mechanisms.

$$0.148 \leq v_f \leq 0.152$$

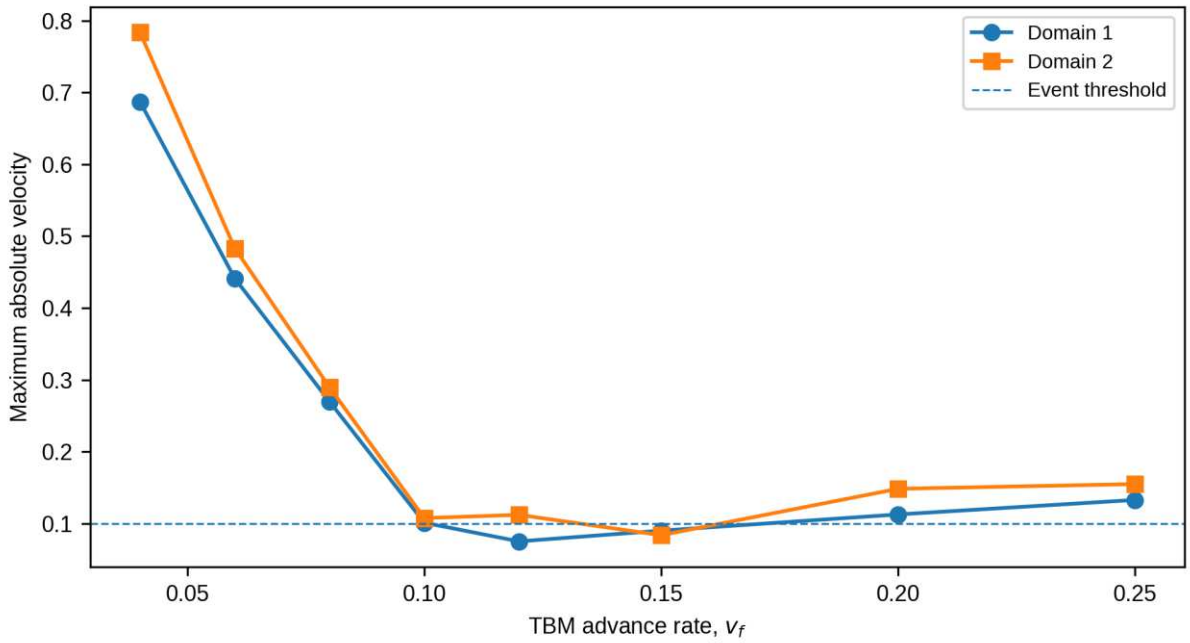


Fig. 4 Non-monotonic peak response versus TBM advance rate

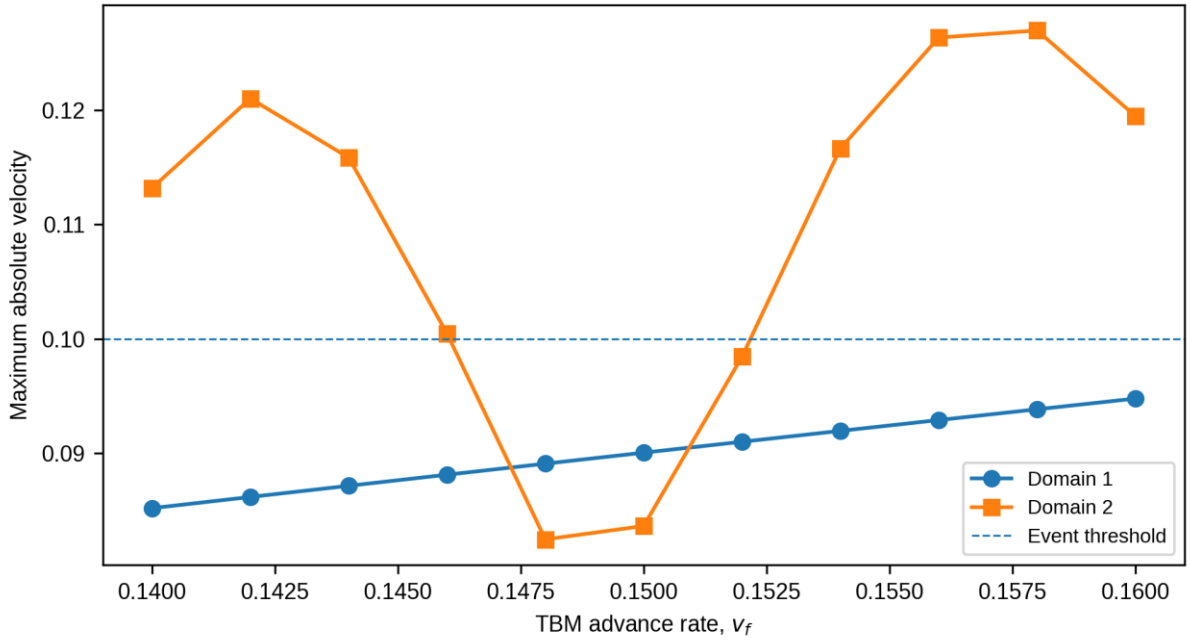


Fig. 5 Local stabilization window around v_f = 0.15

4.5 Influence of interaction delay

The interaction delay produced alternating stability and instability windows. The system remained stable for short delays, became strongly unstable for intermediate delays, returned to a stable state near θ = 3.0, and destabilized again for larger delays. This behavior is characteristic of delay-controlled phase effects.

Unlike the monotonic effect expected from a simple weakening parameter, delay changes the phase relation between the two domains. A delayed coupling force may oppose the current motion and stabilize the system, or arrive in phase with the velocity and reinforce it. This phase dependence explains the alternating stable and unstable windows in the coarse sweep.

The large changes in velocity occur while maximum memory varies only slightly. Delay therefore acts mainly as a dynamic switch applied to an already weakened system. Memory establishes susceptibility, but the phase of delayed interaction determines whether that susceptibility is expressed as observable instability.

θ	max $\lvert y_1 \rvert$	max $\lvert y_2 \rvert$	Events 1	Events 2	Regime
0.00	0.0649	0.0691	0	0	Stable
0.25	0.0646	0.0635	0	0	Stable
0.50	0.1010	0.1075	4	11	Near-critical
0.75	0.3613	0.3866	87	88	Amplified
1.00	0.4667	0.4984	91	91	Amplified
1.50	0.5399	0.5685	90	91	Maximum response
2.00	0.4818	0.5063	84	85	Amplified
3.00	0.0646	0.0836	0	0	Stable window
4.00	0.4956	0.5175	88	89	Second instability
5.00	0.4606	0.4783	81	82	Second instability

An ultrafine sweep resolved the first transition. Both domains remained stable for $\theta \leq 0.494$. Selective activation of the second domain occurred for $0.495 \leq \theta \leq 0.499$, and coupled activation began at $\theta = 0.500$.

The first transition occurs in two stages. The downstream block crosses the event threshold at a slightly smaller delay, creating a narrow selective interval. Only after a further increase in delay does the upstream block activate and the response become coupled. The selective regime is therefore a genuine part of the model dynamics rather than a consequence of coarse parameter spacing.

Immediately beyond the coupled threshold, event count increases much faster than maximum velocity. This rapid expansion of repeated activity marks the onset of a developed delay-amplified regime. From a monitoring perspective, the emergence of repeated downstream events may therefore be more informative than a single increase in peak amplitude.

$$Stable \rightarrow Selective \rightarrow Coupled$$

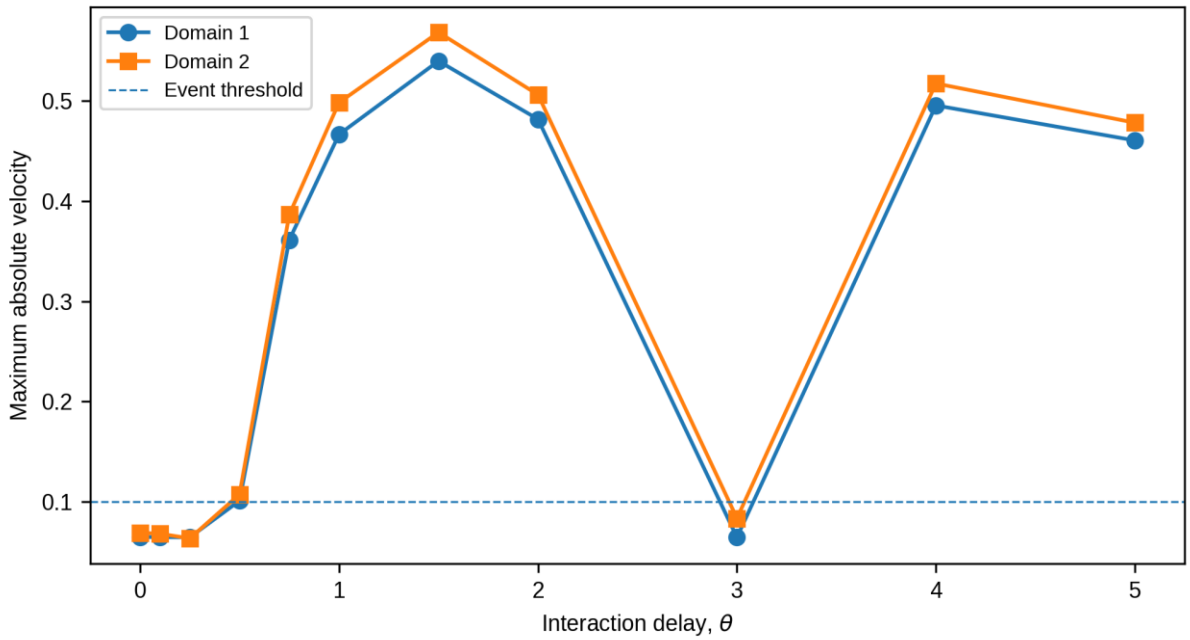


Fig. 6 Alternating delay-controlled stability and instability windows

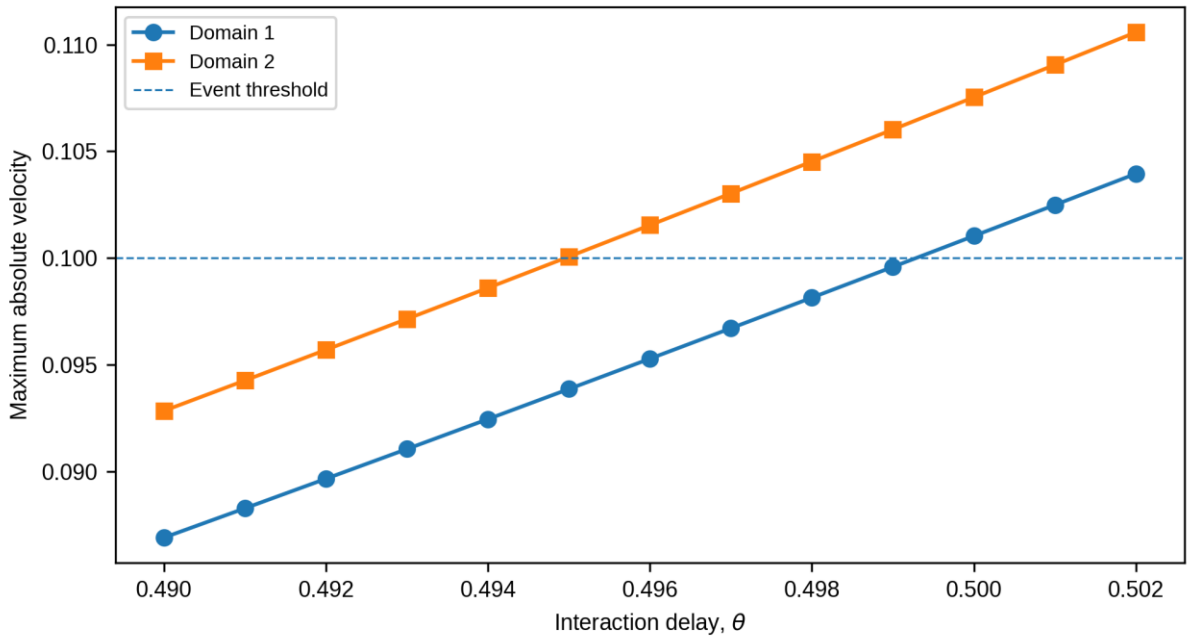


Fig. 7 Ultrafine resolution of selective and coupled delay thresholds

4.6 Influence of memory accumulation and relaxation

4.6.1 Memory accumulation coefficient A

No events occurred for A ≤ 0.01486. The second domain became active at A = 0.01488, and the selective regime persisted to A = 0.01498. Coupled activation occurred at the

baseline value A = 0.01500. Interpolated critical values were A_cr,2 ≈ 0.014868 and A_cr,1 ≈ 0.014981.

The accumulation coefficient controls the rate at which mechanical activity is converted into persistent internal weakening. Below the threshold, substantial memory can accumulate, but the effective friction remains just high enough to prevent delayed coupling from sustaining events. Once the threshold is crossed, the downstream domain activates first and a very small additional increase produces coupled behaviour.

The narrowness of this interval demonstrates that the B1 system is intentionally near critical. It also shows why memory should not be interpreted solely through its absolute value: the mechanical consequence depends on the simultaneous values of gamma, delay, forcing, and coupling stiffness.

$$A_cr, 2 \approx 0.014868, \quad A_cr, 1 \approx 0.014981$$

A	max $\lvert y_1 \rvert$	max $\lvert y_2 \rvert$	Events 1	Events 2	Regime
0.01484	0.09224	0.09842	0	0	Stable
0.01486	0.09332	0.09953	0	0	Stable
0.01488	0.09441	0.10066	0	3	Selective
0.01492	0.09660	0.10292	0	7	Selective
0.01498	0.09992	0.10637	0	10	Selective
0.01500	0.10104	0.10753	4	11	Coupled

For A ≥ 0.030, the unsaturated memory law produced runaway frictional degradation and nonphysical amplitudes. These cases were excluded from the physically interpretable range and motivate the future introduction of residual friction or memory saturation.

This runaway response is a limitation of the present constitutive choice rather than a prediction of physically unlimited rock-mass motion. The exponential weakening law permits the friction scale to approach zero, while the memory equation contains no saturation term. Parameter combinations producing this degeneracy must therefore be excluded, or the model must be extended by residual friction and bounded damage evolution before they can be interpreted physically.

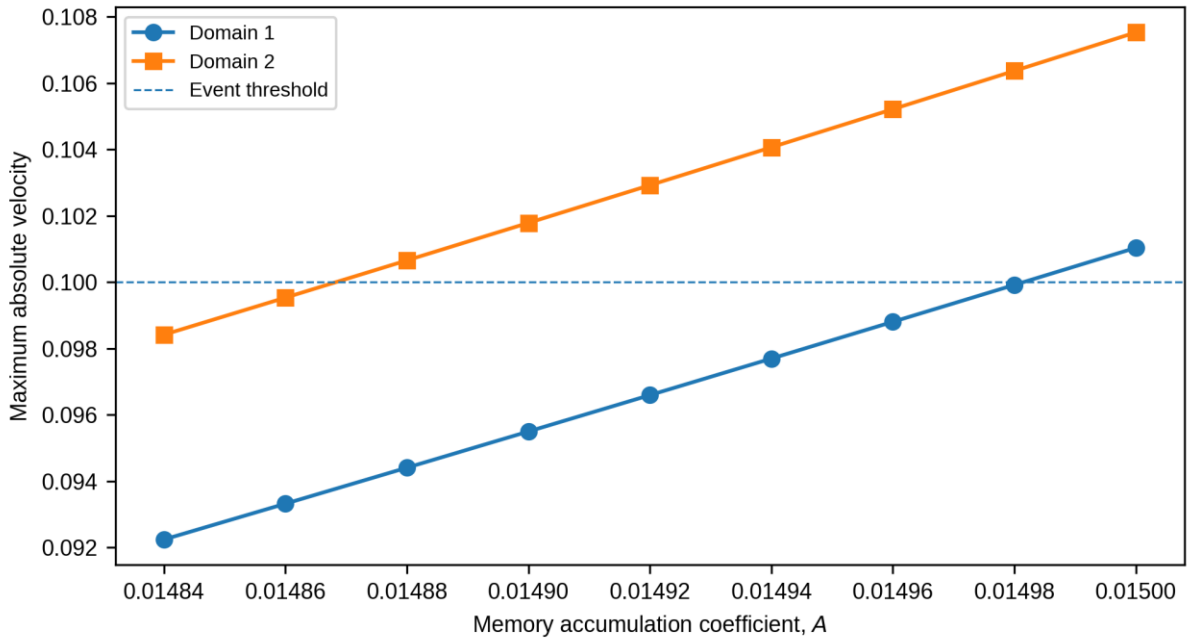


Fig. 8 Ultrafine memory-accumulation threshold

4.6.2 Memory relaxation coefficient B

Increasing B shortened the persistence of the weakened state and stabilized the system. Coupled activity was obtained at B = 0.0050, selective activation at B = 0.0051, and complete stabilization from B = 0.0052. The corresponding characteristic memory times are 200, 196.1, and 192.3, respectively.

The B sweep is the inverse counterpart of the A sweep. Increasing relaxation removes part of the accumulated weakening before delayed coupling can convert it into repeated slip. The system first loses upstream activity, passes through a selective downstream regime, and then becomes fully stable.

The ratio A/B provides a useful summary of the competition between accumulation and recovery, but it is not a universal stability number. Two simulations with the same ratio may still differ if their absolute time scales interact differently with face passage and delay. The separate values of A and B must therefore be retained in project-specific calibration.

B	1/B	max $\|y_1\|$	max $\|y_2\|$	Events 1	Events 2	Regime
0.0050	200.0	0.10104	0.10753	4	11	Coupled
0.0051	196.1	0.09412	0.10047	0	3	Selective
0.0052	192.3	0.08765	0.09396	0	0	Stable
0.0055	181.8	0.07107	0.07737	0	0	Stable
0.0060	166.7	0.06428	0.06273	0	0	Stable

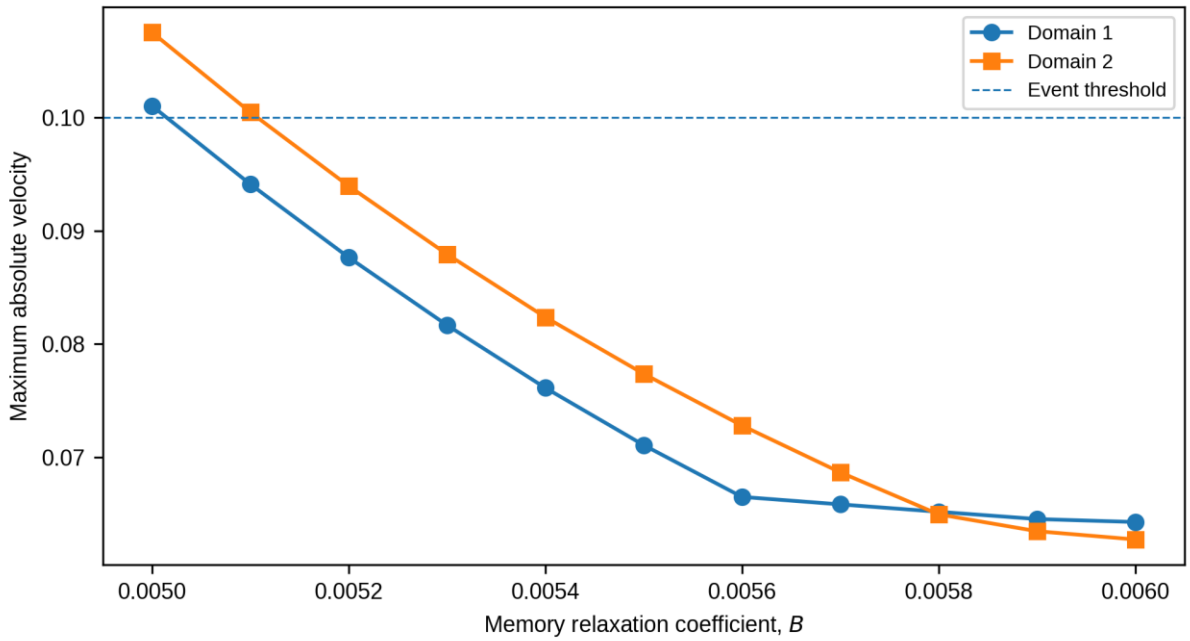


Fig. 9 Fine transition from coupled through selective to stable response

4.7 Friction sensitivity to memory

The parameter γ determines how strongly accumulated memory reduces effective friction. Maximum memory remained nearly unchanged throughout the sweep, so the transition was controlled by the mapping from χ to ρ, rather than by additional damage accumulation.

The gamma sweep isolates the conversion of memory into mechanical weakening because the maximum values of chi remain almost unchanged. The stable-selective-coupled sequence is therefore produced by a change in the efficiency of weakening, not by a change in the amount of accumulated memory.

This observation supports the use of the compound quantity gamma times chi as an indicator of proximity to activation. It should, however, be used together with delayed coupling and excitation measures, because a low friction scale does not by itself guarantee instability when the phase and amplitude of forcing are unfavorable.

$$\rho_i \;=\; exp(-\gamma\chi_i)$$

The ultrafine sweep showed stable behavior for γ ≤ 0.594, selective activation for 0.595 ≤ γ ≤ 0.599, and coupled activity at γ = 0.600. Interpolated critical values were γ_cr,2 ≈ 0.5947 and γ_cr,1 ≈ 0.5993.

γ	max $\|y_1\|$	max $\|y_2\|$	Events 1	Events 2	Regime
0.594	0.09278	0.09897	0	0	Stable
0.595	0.09414	0.10038	0	2	Selective

0.596	0.09550	0.10179	0	5	Selective
0.597	0.09687	0.10321	0	7	Selective
0.598	0.09825	0.10464	0	9	Selective
0.599	0.09964	0.10608	0	10	Selective
0.600	0.10104	0.10753	4	11	Coupled

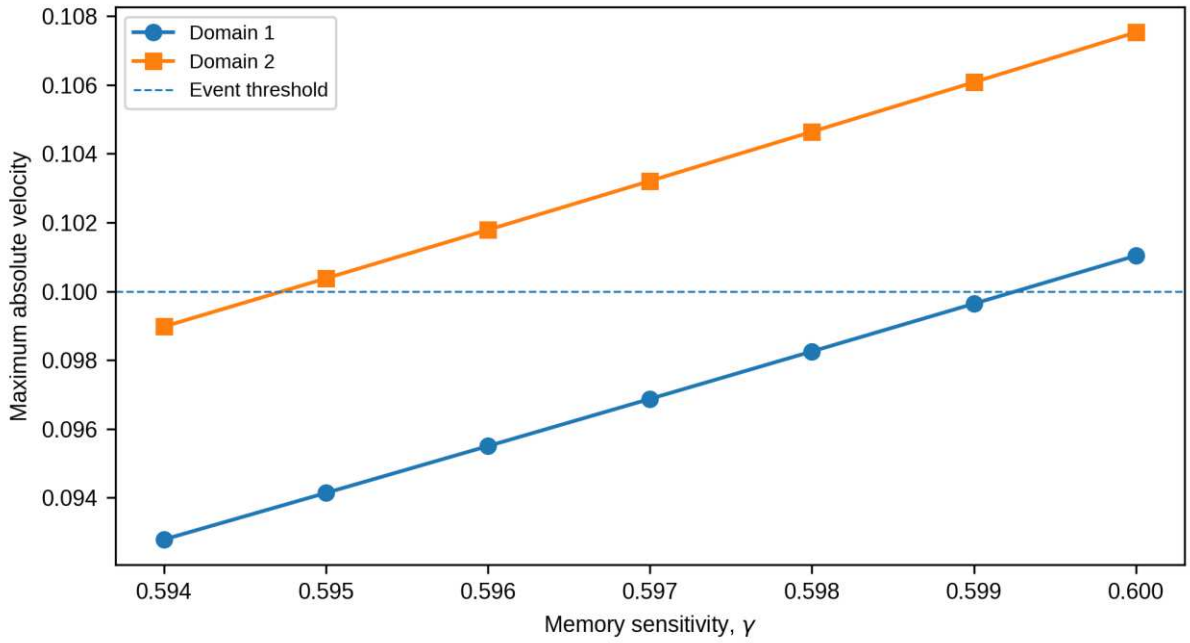


Fig. 10 Ultrafine γ threshold and selective interval

4.8 Global critical parameter space

4.8.1 Unified critical thresholds

The individual sweeps reveal a consistent three-regime topology. Stable response is followed by selective activation of the downstream domain and then by coupled activation of both domains. The critical values are specific to the B1 parameterization, but the repeated transition structure is common to all investigated destabilizing mechanisms.

The numerical thresholds should be read as local boundaries around the selected B1 reference state. They are not independent universal constants: changing stiffness, block spacing, the influence-function shape, or the event threshold would shift their numerical values. Their scientific value lies in the repeated topology of the transition and in the relative ordering of the two domain thresholds.

Parameter	Stable regime	Selective regime	Coupled regime
Forcing p	$p \leq 3.13$	$p = 3.14$	$p \geq 3.15$
Advance rate v_f	0.148–0.152	Adjacent intervals, Block 2 only	$v_f = 0.10$ or $v_f \geq 0.18$

Delay θ	θ ≤ 0.494	0.495–0.499	θ ≥ 0.500 (first window)
Accumulation A	A ≤ 0.01486	0.01488–0.01498	A ≥ 0.01500
Relaxation B	B ≥ 0.0052	B ≈ 0.0051	B ≤ 0.0050
Sensitivity γ	γ ≤ 0.594	0.595–0.599	γ ≥ 0.600

4.8.2 Common transition mechanism

$$Stable \rightarrow Selective\ downstream\ activation \rightarrow Coupled\ delayed\ instability$$

The recurrence of this sequence indicates that selective downstream activation is not a parameter-specific artifact. It is an intrinsic precursor state of the coupled delayed-memory model. The second domain is systematically more sensitive because it experiences its own excavation forcing together with delayed mechanical interaction from the first domain and slightly greater memory accumulation.

The selective regime is especially robust. It appears when destabilization is approached by increasing excitation or weakening, and also when stability is approached by increasing memory relaxation. In every case, the downstream domain remains active over a narrow interval after the upstream domain has become stable, or activates before the upstream domain becomes unstable.

This asymmetry arises from the spatially moving load and the delayed mechanical connection. The second domain receives a compound disturbance: its local excavation forcing and a history-dependent contribution from the first domain. It is therefore not simply a duplicate of the first block at a later time.

4.8.3 Internal weakening and external excitation

The governing parameters separate naturally into internal-weakening variables (A, B, and γ) and external-excitation variables (p, v_f, and θ). Instability requires their interaction. Memory places the system in a weakened state; excavation forcing and delayed coupling determine whether this state is dynamically activated.

Internal weakening and external excitation should be viewed as necessary but individually insufficient conditions. Strong memory degradation can remain dynamically silent when delay is stabilizing, whereas favorable delay cannot generate events when the effective friction remains high. Instability emerges only from their joint configuration.

This interaction explains why single-parameter empirical warning levels may be unreliable. A practical monitoring framework would need to combine machine operation, event timing relative to face position, spatial migration of activity, and indicators of persistent ground degradation.

Parameter group	Parameters	Primary role
Internal weakening	A, B, γ	Accumulation, persistence, and mechanical effectiveness of memory

External excitation	p, v_f, θ	Magnitude, duration, and phase of excavation-induced disturbance
Unified state variable	ρ = exp(−γχ)	Effective frictional resistance available during excitation

4.8.4 Engineering interpretation

Within the model, selective downstream activity is the earliest dynamically observable stage preceding fully coupled instability. This suggests that monitoring strategies should track not only total event counts but also the spatial localization and migration of low-energy activity relative to the excavation face. A transition from isolated downstream events to activation of multiple mechanically connected domains may provide an early indicator of increasing dynamic susceptibility.

The model does not imply that every isolated event ahead of or behind a TBM face is a precursor to failure. The proposed interpretation applies to a systematic transition: repeated or increasing activity localized in a mechanically connected downstream zone, accompanied by evidence that the upstream zone remains subcritical. Field validation would require microseismic locations, TBM operational records, geological structure, and support-installation timing.

Accordingly, the principal engineering contribution is not a direct alarm threshold but a pattern-recognition hypothesis. Spatially selective activation may indicate that excavation history and delayed interaction are bringing the system toward a broader coupled response. This hypothesis can be tested against monitored tunnel sections and used to guide future calibration of the reduced-order model.

4.9 Summary of numerical findings

The simulations demonstrate that moving excavation forcing, nonlinear friction, slow memory evolution, and delayed mechanical coupling generate a rich set of transient regimes. B0 provides a stable reference response. B1 lies immediately beyond multiple critical thresholds and develops delayed clustered stick–slip. The TBM advance rate produces a non-monotonic response with a narrow stabilization window. Delay creates alternating stability and amplification windows. Memory accumulation, relaxation, and sensitivity each generate a two-stage stable–selective–coupled transition. Across all analyses, the selective activation of the second domain emerges as a robust precursor of fully coupled instability.

Taken together, the results support a mechanistic interpretation in which the advancing face creates the loading history, memory preserves part of that history, frictional sensitivity converts it into weakening, and delayed coupling determines whether the weakened state is amplified or suppressed. The observed regimes are therefore products of interaction among processes rather than independent effects of individual parameters.

The reduced figure set emphasizes the transitions that are central to this interpretation. Detailed event-count, energy, memory, and friction curves remain part of the underlying numerical archive, but the chapter focuses on the plots required to establish the stable, selective, and coupled regimes and to explain their physical meaning.

5. Discussion and Engineering Implications

5.1 Interpretation of the principal dynamic regimes

The numerical results demonstrate that the response of the coupled TBM-rock mass system cannot be described by a single monotonic relationship between excavation parameters and instability. Instead, the model produces several distinct regimes whose occurrence depends on the combined effects of excavation forcing, advance rate, delayed mechanical interaction, and memory-dependent frictional weakening.

The stable regime is characterized by bounded transient motion and gradual adjustment of the two rock domains to the passage of the excavation face. Although the displacement and memory variables may increase substantially, the velocity remains below the prescribed event threshold. This regime should not be interpreted as the absence of excavation-induced disturbance. Rather, it represents a condition in which stress redistribution and progressive weakening remain insufficient to generate rapid slip along the modelled discontinuities.

The selective regime represents an intermediate state in which only the second rock domain becomes dynamically active. This regime consistently emerged between the stable and coupled responses when the forcing amplitude, interaction delay, memory accumulation, memory relaxation, or friction sensitivity was varied. Its repeated appearance indicates that selective activation is not an isolated numerical feature, but a characteristic consequence of the asymmetry introduced by the moving excavation front and the delayed coupling between neighbouring domains.

The coupled regime is characterized by activation of both domains and the development of repeated slip events. Near the instability threshold, these events appear as delayed and weakly clustered oscillations. Farther from the threshold, the number of events, peak velocity, and cumulative energy increase rapidly. The transition from selective to coupled behaviour therefore represents a qualitative change in the spatial organization of the response, rather than merely an increase in event amplitude.

These regimes suggest a progressive instability sequence in which excavation-induced disturbance first modifies the internal state of the rock mass, then activates the more sensitive domain, and finally develops into a mechanically coupled response involving multiple neighbouring discontinuities.

5.2 Delayed instability behind the excavation face

One of the most important outcomes of the model is the occurrence of dynamic events long after the excavation face has passed the corresponding rock domain. In the B1 reference case, the first event in the second domain occurred more than one hundred dimensionless time units after local face passage, while activation of the first domain occurred even later.

This delayed response results from the combined action of the slow memory subsystem and delayed mechanical coupling. The excavation forcing reaches its maximum close to the local face-passage time, but the memory variable continues to evolve after the forcing has begun to decay. During this period, the effective frictional resistance progressively decreases according to

$$\rho_i \;=\; exp(-\gamma_i\, \chi_i).$$

Consequently, a discontinuity that remains stable during the peak excavation disturbance may become unstable later, when the direct forcing is weaker but the accumulated mechanical degradation is greater.

In engineering terms, the model indicates that the zone of potential instability cannot be defined exclusively by the instantaneous position of the TBM face. The surrounding rock mass may remain dynamically sensitive behind the excavation front, particularly when damage relaxation is slow or when mechanical interactions between adjacent structural domains are delayed.

This behaviour is relevant to monitoring strategies because localized failures or microseismic events occurring behind the face should not automatically be interpreted as unrelated to excavation. They may represent the delayed manifestation of stress redistribution and cumulative weakening initiated during earlier stages of face advancement.

5.3 Selective downstream activation as a precursor regime

The repeated occurrence of selective activation of the second domain is one of the most consistent findings of the numerical analysis. The second block frequently crossed the event threshold before the first, despite being reached later by the advancing excavation face.

This apparent reversal results from the combined loading history of the downstream domain. The second domain is subjected to its own excavation-induced forcing while also receiving delayed mechanical influence from the first domain. Because the excavation influence zones overlap in space and time, the downstream block may accumulate damage under the combined effects of local forcing and transmitted deformation.

The selective regime may therefore be interpreted as a precursor to fully coupled instability. During this stage, the system remains globally subcritical in the sense that not

all interacting domains are activated, but a localized portion of the rock mass has already entered a dynamic state.

For field monitoring, this result suggests that the spatial distribution of events may be more informative than the total event count alone. A localized increase in activity ahead of or around a particular structural zone could indicate that the system is approaching a coupled transition, even if the overall level of microseismicity remains moderate.

However, the model does not establish a universal warning criterion. The selective regime is defined within a reduced-order dimensionless system and its direct application to a real tunnel would require calibration against structural mapping, stress conditions, TBM operational data, and monitoring records.

5.4 Non-monotonic influence of TBM advance rate

The relationship between TBM advance rate and instability was found to be strongly non-monotonic. Slow advance rates produced intense, memory-dominated stick-slip activity because each rock domain remained within the excavation influence zone for a prolonged period. This extended exposure allowed the memory variable to accumulate and the effective frictional resistance to decrease substantially.

At intermediate advance rates, the system entered a narrow stabilization window. In this interval, the exposure duration was too short for strong memory accumulation, while the rate of mechanical loading remained insufficient to generate an impulsive response.

At higher advance rates, dynamic activity reappeared. In this regime, instability was no longer controlled primarily by cumulative memory but by the rapid temporal variation of the excavation-induced forcing. The response shifted from strongly delayed post-passage activation toward near-face or ahead-of-face events.

The resulting pattern may be summarized as

$$slow\ advance \rightarrow memory-dominated\ instability,$$

$$intermediate\ advance \rightarrow stabilized\ response,$$

$$rapid\ advance \rightarrow impulsive\ instability.$$

This result has an important practical implication: reducing or increasing the advance rate does not necessarily reduce the dynamic response. The effect depends on the relative timescales of excavation loading, damage accumulation, relaxation, and mechanical interaction.

The stabilization interval obtained in the present dimensionless simulations should not be interpreted as a recommended operational TBM velocity. Its significance is conceptual: it demonstrates that an optimal dynamic balance may exist between exposure duration and loading rate. Project-specific application would require dimensional calibration and

consideration of face pressure, penetration rate, support installation, geological conditions, and machine-ground interaction.

5.5 Role of delayed mechanical interaction

The interaction delay was one of the strongest control parameters in the model. The system remained stable for small delays, became unstable near the first critical delay, developed strong repeated slip for intermediate values, returned to a stable state around a secondary delay window, and became unstable again for larger delays.

This alternating sequence of stable and unstable windows indicates that delay modifies the phase relationship between the interacting domains. When the delayed coupling force acts in phase with the current motion, it can reinforce oscillations and promote instability. When it acts out of phase, it may suppress relative movement and stabilize the response.

The delay should not be interpreted as the propagation time of an elastic wave, which would generally be much shorter than the timescales represented in the model. Instead, it is an effective parameter incorporating several slower processes, including:

- progressive fracture propagation;
- redistribution of contact forces;
- delayed mobilization of discontinuity shear resistance;
- time-dependent deformation;
- pore-pressure redistribution;
- delayed influence of support installation or annular grouting.

The existence of multiple stability windows also implies that a longer delay is not necessarily more destabilizing. The response depends on the relation between the delay and the characteristic oscillation timescale of the mechanical subsystem.

This result is particularly relevant for structurally complex rock masses, where separate discontinuity-bounded domains may interact through progressive rather than instantaneous stress transfer.

5.6 Interaction between memory accumulation, relaxation, and frictional sensitivity

The parameters A, B, and γ influence different stages of the same weakening mechanism. The accumulation coefficient A determines how rapidly mechanical activity is converted into the internal memory state. Increasing A leads to faster degradation and earlier activation. The relaxation coefficient B controls how long the weakened state persists. Increasing B reduces the maximum memory, delays the onset of events, and eventually suppresses instability. The sensitivity coefficient γ determines how strongly a given memory state reduces the frictional contribution to the mechanical equations.

Their combined influence is expressed through

$$\rho_i \;=\; exp(-\gamma_i\, \chi_i),$$

with χ_i governed by the competition between accumulation and relaxation.

The results show that the maximum memory alone is not sufficient to characterize stability. Similar values of χ_i may produce either stable or unstable response depending on γ_i. Conversely, the same sensitivity parameter may have little effect when the accumulation rate is low or the relaxation rate is high.

A useful conceptual measure of internal weakening is therefore

$$M_i = \gamma_i \chi_i,$$

or equivalently the effective friction factor ρ_i. These quantities combine the accumulated state and its mechanical significance.

Nevertheless, no universal critical value of ρ_i can be inferred from the present simulations because the instability threshold also depends on forcing, delay, stiffness, and coupling. The friction factor should therefore be regarded as a state indicator rather than an independent failure criterion.

5.7 Internal weakening and external excitation

The results can be interpreted through the interaction of two groups of mechanisms. The first group controls internal weakening:

$$A, \quad B, \quad \gamma.$$

These parameters determine how excavation-induced activity modifies the internal state and effective frictional resistance. The second group controls external excitation:

$$p, \quad v_f, \quad \theta.$$

These parameters determine the magnitude, duration, and phase structure of the mechanical disturbance.

Neither internal weakening nor external excitation alone was sufficient to produce the B1 dynamic regime. Without memory accumulation or friction sensitivity, the system remained stable despite the presence of delayed coupling and excavation forcing. Similarly, substantial memory accumulation did not produce events when the interaction delay remained below its critical range.

This indicates that instability emerges through the coincidence of a sufficiently weakened internal state and a sufficiently destabilizing excitation pattern. The conceptual stability condition may therefore be expressed as

$$\mathcal{I} = \mathcal{W}(A, B, \gamma)\, \mathcal{E}(p, v_f, \theta, \kappa_c),$$

where $\mathcal{W}$ represents internal weakening and $\mathcal{E}$ represents external excitation. Dynamic activation occurs when the combined instability measure $\mathcal{I}$ exceeds a critical level. This expression is conceptual rather than a calibrated engineering criterion, but it provides a useful framework for organizing the effects of the governing parameters.

5.8 Interpretation in relation to TBM monitoring

The principal model variables cannot be directly equated with measured TBM or microseismic quantities without calibration. However, several qualitative correspondences may be proposed.

Sharp velocity peaks may represent rapid slip along discontinuities, localized fracture activation, or low-energy microseismic events. The number and clustering of peaks may be compared qualitatively with event-rate evolution.

The memory variable may be interpreted as a latent state representing cumulative damage, contact degradation, or progressive reduction of discontinuity resistance. It is not directly measurable, but may potentially be inferred from combinations of observable indicators such as:

- cumulative microseismic energy;
- event-rate acceleration;
- increasing apparent volume;
- repeated activation of the same source zone;
- changes in TBM torque and thrust;
- increasing convergence or support loading.

The model predicts that the temporal evolution and spatial migration of activity are more informative than isolated peak values. In particular, the transition from stable to selective and then coupled behaviour suggests that monitoring systems should examine whether activity remains localized or begins to involve multiple interacting zones.

The distinction between delayed post-passage events and ahead-of-face activation is also important. Delayed activity may indicate memory-dominated degradation, whereas ahead-of-face activity may reflect strong mechanical interaction or rapid excitation of a pre-weakened structural zone.

, memory, delay, and nonlinear friction within a transparent dynamical framework.

5.9 Directions for model development and validation

Several extensions are required before the framework can be applied to project-specific prediction. The two-block system may be generalized to a chain or network of N interacting domains. This would allow the study of spatial propagation, migration of activity, and interaction between multiple discontinuity zones.

The excavation forcing function may be derived from analytical solutions or calibrated finite-element simulations of stress redistribution around the TBM face.

The memory law may be modified to include saturation:

$$\dot{\chi}_i = A_i \Phi_i (1 - \chi_i/\chi_max) - B_i \chi_i,$$

and the friction factor may include residual resistance:

$$\rho_i = \rho_res + (\rho_0i - \rho_res)\, exp(-\gamma_i\, \chi_i).$$

These modifications would prevent nonphysical runaway weakening at large damage levels.

Hydraulic effects could be incorporated through an additional pore-pressure variable, allowing the model to represent delayed effective-stress changes in water-bearing fault or fracture zones.

The model parameters could be calibrated using a combination of geological mapping, laboratory joint testing, in situ stress measurements, TBM operational records, convergence monitoring, and microseismic observations.

Validation should focus first on qualitative temporal patterns rather than direct event magnitude prediction. Relevant validation targets include:

- event occurrence before and behind the face;
- delayed event sequences;
- spatial migration of activity;
- event clustering;
- sensitivity to advance rate;
- activation of mapped discontinuity zones;
- changes in response after operational adjustments.

A calibrated version of the model could eventually serve as a reduced-order component within a broader monitoring or digital-twin framework.

5.12 Overall engineering significance

The proposed model provides a complementary perspective to conventional continuum and discontinuum analyses. Detailed numerical models remain necessary for determining stresses, deformations, support demand, and local failure zones. The present framework addresses a different question: how can the time-dependent interaction of excavation forcing, accumulated weakening, and delayed stress transfer generate transitions between stable and dynamically active states?

The results suggest that excavation-induced instability is not controlled by a single parameter or instantaneous stress condition. It emerges from the evolving history of the system.

The most significant model prediction is the repeated appearance of an intermediate selective regime in which the downstream domain becomes active before the full coupled system destabilizes. If a comparable sequence is confirmed in field monitoring data, it could provide a useful conceptual basis for identifying precursor patterns during TBM excavation.

The model should therefore be regarded as a hypothesis-generating and mechanism-oriented framework. Its present value lies in identifying possible dynamic pathways and monitoring indicators, while quantitative engineering application remains dependent on dimensional calibration and field validation.

6. Conclusions

This study developed a reduced-order nonlinear dynamic model for investigating the time-dependent response of jointed rock masses during TBM-driven metro tunnel excavation. The advancing excavation face was represented as a moving mechanical disturbance acting on two coupled rock domains with nonlinear friction, delayed interaction, memory-dependent weakening, and stochastic capability.

The numerical results demonstrated that excavation-induced instability cannot be explained solely by the instantaneous position of the TBM face or by a single governing parameter. Instead, the response emerges from the interaction between external excitation and the evolving internal state of the rock mass.

The stable reference case B0 produced bounded deformation, gradual memory accumulation, and delayed but subcritical velocity peaks. This result confirmed that passage of the excavation face does not necessarily generate dynamic slip, even when the rock mass experiences measurable weakening.

Increasing the excavation forcing produced a sharp transition from stable response to selective activation of the second domain and subsequently to coupled clustered stick-slip. The B1 case, defined by p = 3.15, represented a near-critical state in which both domains became dynamically active after substantial post-passage delays.

The TBM advance rate exerted a strongly non-monotonic influence. Slow advance promoted memory-dominated instability through prolonged exposure, intermediate advance rates produced a narrow stabilization window, and rapid advance generated renewed instability through impulsive loading. For the adopted dimensionless parameter set, the numerically confirmed stable interval was approximately

$$0.148 \leq v_f \leq 0.152.$$

Delayed mechanical coupling was essential for the B1 instability. The system remained stable in the absence of delay and for small values of θ, while coupled activation emerged near θ = 0.50. The delay analysis also revealed alternating stability and instability windows, demonstrating that delayed interaction may either amplify or suppress the response depending on its phase relation with mechanical motion.

Memory accumulation, memory relaxation, and friction sensitivity controlled different stages of the same weakening mechanism. The accumulation coefficient A determined how rapidly damage-related memory developed, the relaxation coefficient B controlled persistence of the weakened state, and γ governed how strongly memory reduced

effective friction. The local transition values obtained for the B1 system were approximately

$$A_cr,2 \approx 0.01487, \quad A_cr,1 \approx 0.01498,$$

$$B_cr,1 \approx 0.00502, \quad B_cr,2 \approx 0.00511,$$

$$\gamma_cr,2 \approx 0.5947, \quad \gamma_cr,1 \approx 0.5993.$$

These values are dimensionless transition points for the adopted B1 parameter set and should not be interpreted as universal physical constants.

All major control parameters produced the same qualitative sequence:

$$stable\ response \rightarrow selective\ downstream\ activation \rightarrow coupled\ instability.$$

The repeated appearance of this sequence suggests that selective activation of the downstream domain is an intrinsic precursor regime of the proposed delayed-memory system. Delayed events behind the excavation face emerged naturally from the interaction of slow memory evolution and delayed coupling, whereas stronger excitation or delay shifted the response toward near-face or ahead-of-face activation.

The maximum memory value alone did not determine stability. Dynamic activation depended on the combined state of frictional weakening, excitation intensity, advance rate, coupling stiffness, and interaction delay. A useful internal-state indicator is the effective friction factor

$$\rho_i = exp(-\gamma_i \chi_i),$$

although no universal critical value of ρ_i can be inferred without dimensional calibration and project-specific validation.

The proposed framework is not intended to replace continuum or discontinuum numerical methods. It provides a complementary approach for examining temporal evolution, delayed activation, event clustering, and transitions between dynamic regimes. Its principal value lies in isolating mechanisms that are difficult to interpret through a sequence of quasi-static excavation stages.

The principal limitations arise from the two-domain idealization, the prescribed excavation influence function, phenomenological friction and memory laws, the dimensionless formulation, and the absence of project-specific calibration. Large values of the memory accumulation coefficient also revealed the need for residual friction and damage saturation in future versions of the model.

Future work should extend the system to multiple interacting domains, introduce bounded memory evolution and residual friction, incorporate hydraulic effects, calibrate the excavation forcing using detailed numerical models, and validate the predicted temporal patterns against TBM operational records and microseismic monitoring data.

Overall, the study demonstrates that moving excavation forcing, delayed stress transfer, and memory-dependent frictional weakening can generate stable, selective, clustered, and strongly coupled dynamic responses within a unified mathematical framework. This provides a conceptual basis for investigating delayed instability and possible precursor patterns during TBM excavation in jointed and faulted rock masses.

Funding

The author received no specific funding for this work.

Author contributions

S.K. conceived the study, developed the model, implemented the numerical simulations, analysed the results, prepared the figures, and wrote and revised the manuscript.

Ethics, Consent to Participate, and Consent to Publish declarations: not applicable

Data availability statement:

Data sets generated during the current study are available from the corresponding author on reasonable request.

References

Doroodian, B., Ahangari, K. and Noorzad, A. (2022). Damage caused by mechanized tunnel boring in high-stress hard rock. Transportation Geotechnics, 34, 100741. https://doi.org/10.1016/j.trgeo.2022.100741

Fan, C., Feng, X.-T., Fu, L., Zhao, J., Yang, C. and Yao, Z. (2023). Evolution law and mechanism of time-delayed spalling in a deep TBM tunnel: A case study. Engineering Geology, 325, 107309. https://doi.org/10.1016/j.enggeo.2023.107309

Fang, X., Yang, J., Zhang, X., Zhang, C., Wang, S. and Xie, Y. (2023). Numerical modeling of open TBM tunneling in stratified rock masses using a coupled FDM-DEM method. Computers and Geotechnics, 156, 105251. https://doi.org/10.1016/j.compgeo.2023.105251

Feng, G.-L., Feng, X.-T., Chen, B.-R., Xiao, Y.-X. and Yu, Y. (2015). Microseismic sequences associated with rockbursts in the tunnels of the Jinping II hydropower station. International Journal of Rock Mechanics and Mining Sciences, 80, 89-100. https://doi.org/10.1016/j.ijrmms.2015.06.011

Kostic, S., Gojkovic, N. and Vasovic, N. (2013). Complex dynamics of a model of mining-generated earthquakes along reactivated faults. Mining and Metallurgy Engineering Bor, 1, 131-140. https://doi.org/10.5937/rudrad1301135K

Li, P.-X., Chen, B.-R., Xiao, Y.-X., Feng, G.-L., Zhou, Y.-Y. and Zhao, J.-S. (2023). Rockburst and microseismic activity in a lagging tunnel as the spacing between twin TBM excavated tunnels changes: A case from the Neelum-Jhelum hydropower project.

Tunnelling and Underground Space Technology, 132, 104884. https://doi.org/10.1016/j.tust.2022.104884

Liu, G., Liu, Z., Feng, G., Chen, X., Duan, S., Liu, C. and Zhao, J. (2025). Disaster characteristics and mechanisms of the time-delayed rockburst development process in tunnels at 2500 m depth. Tunnelling and Underground Space Technology, 159, 106474. https://doi.org/10.1016/j.tust.2025.106474

Ma, T.H., Tang, C.A., Tang, L.X., Zhang, W.D. and Wang, L. (2015). Rockburst characteristics and microseismic monitoring of deep-buried tunnels for Jinping II Hydropower Station. Tunnelling and Underground Space Technology, 49, 345-368. https://doi.org/10.1016/j.tust.2015.04.016

Tang, Z., Liu, X., Xu, Q., Li, C. and Qin, P. (2018). Stability evaluation of deep-buried TBM construction tunnel based on microseismic monitoring technology. Tunnelling and Underground Space Technology, 81, 512-524. https://doi.org/10.1016/j.tust.2018.08.028

Tang, S., Li, J., Tang, L. and Zhang, L. (2023). Microseismic monitoring and experimental study on rockburst in water-rich area of tunnel. Tunnelling and Underground Space Technology, 141, 105366. https://doi.org/10.1016/j.tust.2023.105366

Zhang, Q., Zhang, X.-P., Liu, Q., Chi, J. and Qiu, J. (2023). Microseismic characteristic and development mechanism of fault-slip rockburst in a deep-buried TBM excavated tunnel: A case study. Tunnelling and Underground Space Technology, 142, 105451. https://doi.org/10.1016/j.tust.2023.105451